

This is a repository copy of Alkali-mediated Sr incorporation mechanism and binding capacity of alkali aluminosilicate hydrate in geopolymers.

White Rose Research Online URL for this paper: <a href="https://eprints.whiterose.ac.uk/id/eprint/232884/">https://eprints.whiterose.ac.uk/id/eprint/232884/</a>

Version: Accepted Version

#### Article:

Geddes, D.A. orcid.org/0000-0001-6372-2551, Stennett, M.C., Wilkinson, T.J. orcid.org/0009-0001-0857-7029 et al. (4 more authors) (2025) Alkali-mediated Sr incorporation mechanism and binding capacity of alkali aluminosilicate hydrate in geopolymers. Journal of Hazardous Materials, 488, 137426. ISSN: 0304-3894

https://doi.org/10.1016/j.jhazmat.2025.137426

© 2025 The Authors. Except as otherwise noted, this author-accepted version of a journal article published in Journal of Hazardous Materials is made available via the University of Sheffield Research Publications and Copyright Policy under the terms of the Creative Commons Attribution 4.0 International License (CC-BY 4.0), which permits unrestricted use, distribution and reproduction in any medium, provided the original work is properly cited. To view a copy of this licence, visit http://creativecommons.org/licenses/by/4.0/

### Reuse

This article is distributed under the terms of the Creative Commons Attribution (CC BY) licence. This licence allows you to distribute, remix, tweak, and build upon the work, even commercially, as long as you credit the authors for the original work. More information and the full terms of the licence here: https://creativecommons.org/licenses/

#### **Takedown**

If you consider content in White Rose Research Online to be in breach of UK law, please notify us by emailing eprints@whiterose.ac.uk including the URL of the record and the reason for the withdrawal request.



# Alkali-mediated Sr incorporation mechanism and binding capacity of

# alkali aluminosilicate hydrate in geopolymers

Daniel A. Geddes<sup>1†</sup>, Martin C. Stennett<sup>1†</sup>, Tom J. Wilkinson<sup>1</sup>, Benjamin E. Griffith<sup>2</sup>, John V. Hanna<sup>2</sup>, John
 L. Provis<sup>3</sup>, Brant Walkley<sup>1\*</sup>

<sup>1</sup>School of Chemical, Materials and Biological Engineering, The University of Sheffield, Sheffield S1 3JD, UK

<sup>2</sup>Department of Physics, The University of Warwick, Coventry, CV4 7AL, UK

<sup>3</sup>PSI Center for Nuclear Engineering and Sciences, Paul Scherrer Institut, Forschungsstrasse 111, 5232 Villigen PSI,

8 Switzerland

Corresponding author: Email: b.walkley@sheffield.ac.uk

10 <sup>†</sup> These authors contributed equally

# **Abstract**

Geopolymers are promising materials for safe immobilisation and disposal of complex radioactive waste streams. This work investigates the effect of Sr incorporation and alkali-activator chemistry on 1) geopolymer chemistry, phase assemblage and nanostructure, 2) chemical binding mechanism of  $Sr^{2+}$  into the aluminosilicate framework of (N,K)-A-S-H gels in geopolymers, and 3) mass transport of  $Sr^{2+}$  during leaching, using high-field solid-state nuclear magnetic resonance spectroscopy and synchrotron-based X-ray absorption spectroscopy measurements. All geopolymers studied comprise a fully polymerised, X-ray amorphous Al-rich (N,K)-A-S-H type gel. Si exists predominantly in tetrahedral  $Q^4$ (4Al) and  $Q^4$ (3Al) sites and Al exists in tetrahedral sites, resulting in a net negative charge that is balanced by  $Na^+$  and/or  $K^+$  in extra-framework sites.  $Sr^{2+}$  was incorporated into extra-framework sites within (N,K)-A-S-H gels, without altering the local structure of the aluminosilicate framework by directly substituting for both  $Na^+$  and  $K^+$  in charge-balancing sites to form a (N,K,Sr)-A-S-H gel, at loadings equal to or below Sr/Na = 0.005. Above this limit,  $SrCO_3$  is formed, and the geopolymers simultaneously chemically bind Sr within a (N,Sr,K)-A-S-H gel, and physically encapsulate excess Sr as  $SrCO_3$ . These findings have significant implications for use of geopolymers as materials for encapsulation and/or immobilisation of radioactive waste containing Sr

#### 1 Introduction

Cementation has received particular attention as a potentially viable method for encapsulation and immobilisation of radioactive waste bearing strontium-90 ( $^{90}$ Sr), a fission product that is present in many radioactive waste streams, including in nuclear reactor cooling water. [1-3] This is due to the relatively short half-life of  $^{90}$ Sr ( $T_{1/2}$  = 28.80 years), which means that  $^{90}$ Sr-bearing cement wasteforms are only required to be durable and secure for on the order of a few hundred years, as well as the compatibility of cement wasteforms with many granular ion exchange materials [4, 5], which are necessary to extract  $^{90}$ Sr from nuclear reactor cooling water, or from remediation of decommissioned or damaged nuclear facilities (e.g. Fukushima Daiichi Nuclear Power Station), and must subsequently be conditioned prior to disposal [6].

Portland cement has traditionally been used for cementation of radioactive waste containing strontium, to act as an additional physical containment barrier. However, hardened Portland cement comprises numerous hydrate phases and high water content, and as a result Sr<sup>2+</sup> uptake is via reversible ion-exchange interactions in phases such as calcium silicate hydrate (C-S-H) [7, 8], which has implications for the resistance of PC wasteforms to leaching, and retention of <sup>90</sup>Sr.

Geopolymers exhibit high potential as suitable materials for radioactive waste cementation due to their cation-binding sites, mechanical properties, enhanced chemical resistance in aggressive environments, and enhanced chemical tolerance to problematic wastes [9-11]. Geopolymers also exhibit desirable flow characteristics in the fresh state, which may potentially enable higher waste loadings and the ability to encapsulate greater volumes of wastes [12-15].

The main binding phase in geopolymers is a structurally disordered and pseudo-zeolitic alkali aluminosilicate framework [16]. The most common alkalis used to produce geopolymers are Na and K, and so the alkali aluminosilicate hydrate gel framework is often abbreviated as (N,K)-A-S-H. Si exists in tetrahedral  $Q^4(mAl)$  sites ( $1 \le m \le 4$ ), while Al is primarily in tetrahedral  $Q^4(4Si)$  sites as a result of the avoidance of  $AI^{IV}$ -O- $AI^{IV}$  bonding [17]. Alkali cations are present in octahedrally coordinated sites, and balance the negative charge arising from Al within tetrahedral sites.

We have previously reported successful chemical immobilisation of Sr in alkali aluminosilicate (geopolymer) gels [18] at concentrations relevant for cementation of radioactive ion exchange resins [19, 20] (up to 0.012 wt. % of the total sample mass and 0.026 mol % of the total Na). Others have reported incorporation of 1-2 mol. % [21, 22], while further studies have shown successful physical encapsulation

of Sr-loaded adsorbents [23-25] in geopolymers. Despite this, the radionuclide incorporation processes which control long-term wasteform performance remain unclear. In particular, 1) there has been little investigation of the upper waste loading limit achievable for chemical immobilisation of Sr in sodium aluminosilicate hydrate gels in geopolymer wasteforms, 2) a detailed understanding of the Sr incorporation in potassium-based geopolymer gels is not yet available, and 3) the role of the alkali cation type and waste loadings achievable in Sr-bearing geopolymer wasteforms remains unknown.

Here, we use multinuclear solid state NMR probing <sup>23</sup>Na, <sup>39</sup>K, <sup>27</sup>Al and <sup>29</sup>Si, including high-field (20.0 T) <sup>39</sup>K MAS and <sup>27</sup>Al MAS and 3QMAS NMR experiments, and synchrotron X-ray absorption measurements, to show for the first time that the incorporation mechanism and chemical binding of Sr<sup>2+</sup> and Ca<sup>2+</sup> into the aluminosilicate framework of (N,K)-A-S-H gels in geopolymer is controlled by the alkali ion type, and to determine the Sr-binding capacity in N-A-S-H gels, and Sr mass transport properties, in these cements. These findings have significant implications for the long-term durability of geopolymers, and show that when formulating geopolymer wasteforms, selection of the alkali ion type in the alkali activator is critical in determining wasteform properties and performance.

# 2 Experimental methods

# 2.1.1 Sample preparation

# 2.1.1.1 Assessing the Sr binding capacity in sodium aluminosilicate hydrate

To assess the effect of Sr loading on the chemical immobilisation mechanism in geopolymer cements, metakaolin (MetaMax, BASF, UK, chemical composition provided in Table 1,  $D_{50}$  = 4.49 µm) was reacted with a solution of sodium silicate containing varying amounts of Sr (added as Sr(OH)<sub>2</sub>·8H<sub>2</sub>O).

Table 1: MetaMax metakaolin chemical composition (wt.%) as determined by X-ray fluorescence analysis
 (LOI: loss on ignition at 1000 °C).

SiO <sub>2</sub>	Al <sub>2</sub> O <sub>3</sub>	K <sub>2</sub> O	Na₂O	MgO	CaO	TiO <sub>2</sub>	Fe <sub>2</sub> O <sub>3</sub>	Other	LOI
52.5	44.5	0.2	0.2	<0.05	<0.05	1.3	0.4	0.2	0.6

Activating solutions were produced by dissolution of sodium hydroxide powder (AnalaR 99 wt.%) in PQ-NS sodium silicate solution (PQ UK,  $SiO_2/M_2O = 2.1$ , 44.1 wt.% sodium silicate with the balance water) and distilled water. Samples were formulated with the chemical composition and water/solids (w/s) ratios shown in Table 2, and an activating solution modulus of  $SiO_2/Na_2O = 1$ .

**Table 2:** Chemical composition (molar basis), and Sr(OH)<sub>2</sub>.8H<sub>2</sub>O content (mass basis) of the reaction mixtures.

Sample code	Sr(OH) <sub>2</sub> .8H <sub>2</sub> O content (wt. %)	Si/Al	Na/Al	Sr/Al	Sr/Na	H₂O/Na₂O	w/s
Sr_0.0	0.0	1.35	1.05	0.000	0.000	13.0	0.4
Sr_0.5	0.5	1.35	1.05	0.009	0.005	13.0	0.4
Sr_1.0	1.0	1.35	1.05	0.018	0.009	13.0	0.4
Sr_1.5	1.5	1.35	1.05	0.026	0.013	13.0	0.4
Sr_2.0	2.0	1.35	1.05	0.035	0.018	13.0	0.4
Sr_2.5	2.5	1.35	1.05	0.044	0.022	13.0	0.4
Sr_3.0	3.0	1.35	1.05	0.053	0.027	13.0	0.4

Sr\_3.5 3.5 1.35 1.05 0.062 0.031 13.0 0.4

The activating solution was mixed with metakaolin with a high-shear mixer at 1300 rpm for 10 minutes, and the geopolymer paste was then cast in sealed containers and cured for 28 days at  $20^{\circ}\text{C} \pm 2^{\circ}\text{C}$ . Samples containing natural abundance proportions of the isotopes of  $\text{Sr}^{2+}$  were produced by mixing  $\text{Sr}(\text{OH})_2 \cdot \text{8H}_2\text{O}$  (Sigma Aldrich) with the activating solution and metakaolin to obtain Sr concentrations of up to 3.5 wt. % of the total sample mass and 3.0 mol % of the total Na content in the sample.

# 2.1.1.2 Assessing the effect of the alkali cation on the chemical immobilisation mechanisms

To assess the effect of the alkali cation on the chemical immobilisation mechanisms in geopolymer cements, metakaolin (MetaStar 501, Imerys, chemical composition provided in Table 3) was reacted with a solution of either sodium silicate, potassium silicate, or a blend of sodium and potassium silicate (1:1 molar ratio) to form geopolymer cements.

**Table 3:** MetaStar 501 metakaolin chemical composition (wt.%) as determined by X-ray fluorescence analysis (LOI: loss on ignition at 1000°C).

SiO <sub>2</sub>	$Al_2O_3$	K <sub>2</sub> O	Na₂O	MgO	CaO	TiO <sub>2</sub>	Fe <sub>2</sub> O <sub>3</sub>	Other	LOI
52.6	44.4	0.2	0.3	< 0.05	< 0.05	1.0	0.6	0.0	0.8

Alkali solutions were produced by dissolution of either powdered sodium hydroxide (AnalaR 99 wt.%), powdered potassium hydroxide (AnalaR 99 wt.%), or a combination, in PQ-NS sodium silicate solution PQ UK,  $SiO_2/M_2O = 2.1$ , 44.1 wt.% sodium silicate with the balance water) or PQ-KS potassium silicate solution (PQ UK,  $SiO_2/M_2O = 2.2$ , 51.6 wt.% potassium silicate with the balance water, PQ UK) and distilled water. Samples were formulated with Si/Al = 1.5 ( $SiO_2/Al_2O_3 = 3$ ) and  $M_2O/H_2O = 11$ , w/s = 0.4, an activating solution modulus of  $SiO_2/M_2O = 1$  (where M represents Na and/or K), and the chemical composition shown in Table 4.

**Table 4:** Nominal chemical composition (molar basis) of the alkali activating solution.

			Mole fraction		
Sample Code	Sr/Al	Ca/Al	K₂O	Na₂O	
Na	0	0	0.0	1.0	
Na.K	0	0	0.5	0.5	
K	0	0	1.0	0.0	
Na-Sr	0.00025	0	0.0	1.0	

Na.K-Sr	0.00025	0	0.5	0.5
K-Sr	0.00025	0	1.0	0.0
Na-Ca	0	0.00025	0.0	1.0
Na.K-Ca	0	0.00025	0.5	0.5
K-Ca	0	0.00025	1.0	0.0

Metakaolin was mixed with the activating solution, cast in sealed containers and cured for 3 months at  $20^{\circ}\text{C} \pm 2^{\circ}\text{C}$ . Samples containing  $\text{Ca}^{2+}$  and  $\text{Sr}^{2+}$  were prepared by dissolving  $\text{Sr}(\text{OH})_2 \cdot \text{8H}_2\text{O}$  (Sigma Aldrich) and  $\text{Ca}(\text{OH})_2$  (Sigma Aldrich) in the activating solution and then mixing with metakaolin to obtain ME/Al = 0.00025 (ME =  $\text{Sr}^{2+}$  or  $\text{Ca}^{2+}$ ). Previous work utilising X-ray diffraction data showed that trace amounts of the crystalline phases anatase (TiO<sub>2</sub>), quartz (SiO<sub>2</sub>) and hydroxylated muscovite (illite-2, (K,H<sub>3</sub>O)(Al,Mg,Fe)<sub>2</sub>(Si,Al)<sub>4</sub>O<sub>10</sub>[(OH)<sub>2</sub>,(H<sub>2</sub>O)] were also observed in each geopolymer cement, due to their presence in metakaolin [18]. The hardened binders were hand ground using a mortar and pestle, immersed in acetone for 15 min to remove loosely bound water and to halt the alkali-activation reaction [26]). The ground binders were subsequently filtered and stored in a sealed desiccator under vacuum, prior to characterisation.

# 2.1.1.3 Assessing the Sr mass transport properties using leaching tests

Samples containing between 0 wt. % and 3 wt. %  $Sr(OH)_2 \cdot 8H_2O$  were prepared to assess the mass transport properties of Sr in geopolymers using leaching tests. For these samples stoichiometry was designed to obtain an activating solution modulus of  $SiO_2/Na_2O = 1$  and the nominal chemical composition and water/solids (w/s) ratios outlined in Table 5. To easily distinguish between the samples discussed in this study, they will be referred to in the form  $Y - M_X$ , where Y is the sample identifier (A-H for the eight sample types), M is the alkali cation (either K or M) and M is the percentage by mass of M0 in the sample (ranging from M1 wt. %).

**Table 5:** Chemical composition (molar basis), and Sr(OH)<sub>2</sub>.8H<sub>2</sub>O content (mass basis) of the reaction mixtures.

Sample	Sr(OH) <sub>2</sub> (wt. %)	Si/Al	K/AI	Na/Al	Sr/Al	Sr/(Na+K)	H₂O/Na₂O	w/s
A – K_0%	0.0	1.35	1.05	-	0.000	0.000	13.0	0.4
B – K_1%	1.0	1.35	1.05	-	0.018	0.009	13.0	0.4

C – K_2%	2.0	1.35	1.05	-	0.035	0.018	13.0	0.4
D – K_3%	3.0	1.35	1.05	-	0.053	0.027	13.0	0.4
E – Na_0%	0.0	1.35	-	1.05	0.000	0.000	13.0	0.4
F – Na_1%	1.0	1.35	-	1.05	0.018	0.009	13.0	0.4
G – Na_2%	2.0	1.35	-	1.05	0.035	0.018	13.0	0.4
H – Na_3%	3.0	1.35	-	1.05	0.053	0.027	13.0	0.4

Leach tests were performed according to ANSI/ANS 16.1-2003 [27]. This semi-dynamic leach experiment involves submerging a monolithic, cylindrical sample of fixed geometry into water at a fixed liquid volume to monolith surface area ratio, and replacing the entire leachate volume at given time intervals. Hardened geopolymer wasteforms cured for 28 days at  $20^{\circ}\text{C} \pm 2^{\circ}\text{C}$ , with mass  $4 \text{ g} \pm 0.25 \text{ g}$ , were cast in cylindrical containers to form cylinders 13 mm in diameter and 20 mm  $\pm$  2 mm in length [27]). The ends of each cylindrical sample were sealed with cold setting epoxy to inhibit axial mass transfer. Consequently, it was assumed that two dimensional radial mass transport is the dominant mass transfer mechanism controlling Sr mobility. This assumption allows modelling of the long term leaching of Sr from the geopolymer wasteform in two dimensions, and calculation of diffusion coefficients and leachability indices, as described below.

The hardened samples (sealed at each end with epoxy) were immersed in 79.8 ml  $\pm$  1 ml of deionised water, to provide a strong driving force for leaching of Sr. At 2, 7, 24, and 72 hours, and 7, 14, 21, and 28 days after initial submersion, each sample was removed from the solution and placed in fresh deionised water. At each time point, the sample was washed with deionised water for 30 seconds. This 'wash-off' was combined with the leachate for analysis, as described below. At the end of the 28-day leach test, each sample was removed from solution and subsequently submerged in isopropanol (IPA) to dry the sample and remove any loosely bound water through solvent exchange. The IPA was changed at 8, 24, and 72 hours, and 7 and 14 days, after which the solid samples were prepared for characterisation, as described below.

A Mettler Toledo benchtop digital pH meter was used to measure the pH of the leachate at each time point. Three replicates were measured at each time point. Inductively coupled plasma optical emission spectroscopy (ICP-OES) data were obtained using a Spectro-Ciros-Vision ICP-OES instrument and used to

- determine the concentrations of K, Na, Al, Si, and Sr in the leachate for each sample at each time point.
- 152 Three replicates were measured at each time point.

#### 2.1.2 Characterisation of the geopolymer samples

#### 2.1.2.1 X-ray diffraction

153

154

160

164

- 155 X-ray diffraction (XRD) data were acquired using a Panalytical X'Pert<sup>3</sup> Powder X-ray diffractometer with
- 156 Cu Kα radiation (1.54 Å), a nickel filter, a step size of 0.020° and a count time of 1 s/step, across a 2 $\theta$  range
- of 5°-70°. An anti-scatter blade was used to reduce low angle diffracted background intensity, and an
- incident beam divergence of 1.0 mm and a 2.5° Soller slit in the diffracted beam were used. Phase
- identification was performed using the ICDD PDF4+ 2015 database and Diffrac.EVA V4.1 software.

# 2.1.2.2 Fourier transform infrared spectroscopy

- 161 FTIR spectroscopy data were acquired using a Perkin Elmer Frontier Mid FT-IR spectrometer equipped
- with a deuterated triglycine sulfate (DTGS) detector and KBr beam splitter optical system, scanning 16
- times at a resolution of 4 cm<sup>-1</sup>. Data were acquired for pellets comprising 200 mg KBr with 2 mg of sample.

# 2.1.2.3 Solid state nuclear magnetic resonance spectroscopy

- Solid-state single pulse <sup>29</sup>Si and <sup>23</sup>Na magic angle spinning (MAS) NMR data were acquired at 11.7 T on a
- 166 Bruker Avance III HD 500 spectrometer operating at Larmor frequencies 99.35 MHz and 132.29 MHz,
- respectively. A Bruker 4.0 mm dual resonance CP/MAS probe and MAS frequency of 12.5 kHz was used.
- 168 <sup>29</sup>Si MAS NMR spectra were acquired using a 5.5  $\mu$ s  $\pi/2$  excitation pulse, a measured 90 s relaxation delay,
- a total of 256 FIDs per spectrum. <sup>1</sup>H-<sup>29</sup>Si cross-polarisation (CP) MAS NMR measurements were acquired
- using a  $^{29}$ Si  $\pi/2$  pulse width of 1.7  $\mu$ s, an initial  $^{1}$ H non-selective ( $\pi/2$ ) pulse width of 2.5  $\mu$ s, a recycle delay
- of 1.5 s, a contact pulse of 1.7 ms, and a nominal <sup>1</sup>H decoupling field strength of 80 kHz, with 10240 scans
- 172 collected per experiment. <sup>23</sup>Na MAS NMR data were acquired using a 3  $\mu$ s non-selective ( $\pi$ /2) excitation
- pulse, a measured 10 s relaxation delay and 128 scans per experiment. All <sup>29</sup>Si and <sup>23</sup>Na data were
- 174 referenced to the IUPAC primary references, pure tetramethylsilane (TMS) ( $\delta_{iso}$  = 0 ppm) and 1.0 M
- aqueous NaCl<sub>(aq)</sub> ( $\delta_{iso}$  = 0 ppm), respectively [28].
- Single pulse <sup>27</sup>Al MAS data were acquired at 9.4, 14.1 and 20.0 T using Bruker Avance III HD, Bruker Avance
- Neo 600 and 850 spectrometers operating at the Larmor frequencies 104.23, 156.34 and 221.49 MHz,
- 178 respectively. A 3.2 mm HXY probe and a spinning frequency of 20 kHz was used. Pulse calibration and

chemical shift referencing were carried out using the IUPAC primary reference of 1.1 M solution Al(NO<sub>3</sub>)<sub>3</sub> ( $\delta_{iso}$  = 0 ppm) [28]. A 'non-selective' 18  $\mu$ s  $\pi$ /2 pulse was measured, allowing for a 'selective' 1  $\mu$ s  $\pi$ /12 to be implemented. A minimum of 2600 scans were acquired per spectrum, with a recycle delay of 1 s between subsequent acquisitions. 2D <sup>27</sup>Al 3QMAS z-filter experiments were attained at 20.0 T ( $v_0$  = 221.49 MHz) using a Bruker Avance Neo spectrometers. A 4 pulse z-filter 3QMAS pulse sequence (excitation -conversion -  $\pi$ /2 -  $\pi$ /2 - acquire) was implemented where a calibrated 6.2  $\mu$ s 'hard' excitation pulse, 1.8  $\mu$ s conversion pulse and 11  $\mu$ s 'soft' z-fillter pulses. A total of 64 slices were acquired per spectrum and 96 scans were obtained per slice.

High-field solid state <sup>39</sup>K MAS NMR data were acquired at 20.0 T ( $v_0$  = 39.67 MHz) using a Bruker Avance Neo 850 spectrometer with a Bruker 4.0 mm HX MAS probe, which enabled a spinning rate of 14 kHz to be implemented. Pulse calibration and chemical shift referencing for all <sup>39</sup>K data were achieved using KCl<sub>(s)</sub> ( $\delta_{iso}$  = 47.8 ppm) as a secondary reference to the IUPAC primary reference of 0.1 M KCl<sub>(aq)</sub> ( $\delta_{iso}$  = 0 ppm) [28]. A 'non-selective'  $\pi$ /2 pulse of 12  $\mu$ s was measured allowing for a 'selective' 4  $\mu$ s  $\pi$ /3 to be implemented. Spectra were acquired using a Hahn echo pulse sequence ( $\pi$ /2 –  $\tau$  –  $\pi$  – acquire) using a measured relaxation delay of 0.1 s and acquiring a total of 480,000 transients per spectra.

<sup>29</sup>Si MAS and <sup>1</sup>H-<sup>29</sup>Si CP MAS NMR data were deconvoluted using Gaussian peak distributions [29]. The isotropic chemical shift ( $\delta_{iso}$ ) and peak full width at half maximum (FWHM) of each fitted peak were required to be consistent in both <sup>29</sup>Si MAS NMR and <sup>1</sup>H-<sup>29</sup>Si CP MAS NMR deconvolutions, and the minimum number of peaks possible were fitted. Intensities of the fitted Gaussian distributions were constrained by the thermodynamics of a statistical distribution of Si and Al sites within a Q<sup>4</sup> aluminosilicate network for (N,K)-A-S-H products [17]. Congruent dissolution was assumed in all samples to enable suitable constraints on the spectral deconvolutions, and a scaled spectrum calculated from <sup>29</sup>Si and <sup>27</sup>Al MAS NMR data of unreacted metakaolin was used in the fits to account for the contribution to the data from <sup>29</sup>Si sites within unreacted metakaolin.

### 2.1.2.4 X-ray absorption spectroscopy

XAS data were acquired at Diamond Light Source, Harwell, UK, on the bending magnet beamline B18, using a collimating mirror, a fixed-exit double crystal Si(111) monochromator, and a double toroidal focussing mirror. Sr K-edge XAS data were acquired in transmission mode using finely ground powder samples dispersed in polyethylene glycol to achieve a thickness of one absorption length. Incident and transmitted beam intensities were measured using ionization chambers, filled with mixtures of He and Ar

or N<sub>2</sub>, operated in a stable region of their I/V curve. Yttrium foil was measured to provide an absolute energy calibration; the first inflection point (in the first derivative) was defined to be 17133 eV. The yttrium foil was measured periodically to ensure that there was no energy drift over the course of the experiment. Data reduction and analysis was performed using the programmes Athena, Artemis and Hephaestus [30].

#### 3 Results and discussion

218

219

220

221

222

223

224

225

226

227

228

229

230

231

232233

234

235

236

237

238

239

240

241

242

243

244

# 3.1 Sr binding capacity in sodium aluminosilicate hydrate

# 3.1.1 X-ray diffraction

XRD data for each of the samples produced to assess the effect of the Sr loading on the chemical immobilisation mechanism, as well as that for metakaolin used, are shown in Figure 1. Data for metakaolin (Raw MK) exhibits a large broad feature centred at approximately 22° 20 due to diffuse scattering. This is consistent with the crystallographically disordered nature of metakaolin [31]. Reflections due to anatase (TiO<sub>2</sub>, Powder Diffraction File (PDF) # 01-071-1166), quartz (SiO<sub>2</sub>, PDF # 01-078-1252), and mullite (Al<sub>6</sub>Si<sub>2</sub>O<sub>13</sub> (PDF) # 04-012-0161) are also observed in the XRD data for metakaolin, and are attributed to impurities present, consistent with previous observations [32]. XRD data for each geopolymer gel exhibit a dominant broad feature at approximately 29° 20 due to diffuse scattering, indicating a crystallographically disordered reaction product, consistent with the formation of a sodium aluminosilicate hydrate (N-A-S-H) gel [18, 33, 34]. Reflections due to strontium carbonate (SrCO₃, PDF # 00-005-0418) are also observed in the XRD data for geopolymer gels containing ≥1.5 wt. % Sr(OH)<sub>2</sub>·8H<sub>2</sub>O. The formation of SrCO<sub>3</sub> is consistent with reaction of excess Sr<sup>2+</sup> in the pore solution with atmospheric CO<sub>2</sub> during sample preparation and analysis. Previous work [18] has shown incorporation of Sr content in geopolymers at up to 0.012 wt. % of the total sample mass and 0.026 mol % of the total Na, by chemical binding (immobilisation) of Sr<sup>2+</sup> in charge balancing sites within the N-A-S-H gel (i.e. via formation of a (N,Sr)-A-S-H gel) [18]. The formation of SrCO<sub>3</sub> suggests that 1.3 mol. % of the Na<sup>+</sup> can be replaced by Sr<sup>2+</sup> (equivalent to ≥1.5 wt. % Sr(OH)<sub>2</sub>·8H<sub>2</sub>O in the reaction mixture), and that this is the upper bound on incorporation of Sr within the (N,Sr)-A-S-H gel framework. The mechanisms leading to this upper limit on Sr incorporation limit may be related to the extent to which the local gel structure can accommodate charge balancing cations with different charge states and ionic radii, or may be due thermodynamically or kinetically preferential formation of SrCO₃ compared to (N,Sr)-A-S-H under the reaction conditions used. The XRD data for each geopolymer show reflections due to anatase and quartz, indicating that these are inert throughout the reaction process. This is consistent with the small amount of unreacted metakaolin observed by solid-state MAS NMR in all geopolymer samples (discussed in section 3.1.3.).

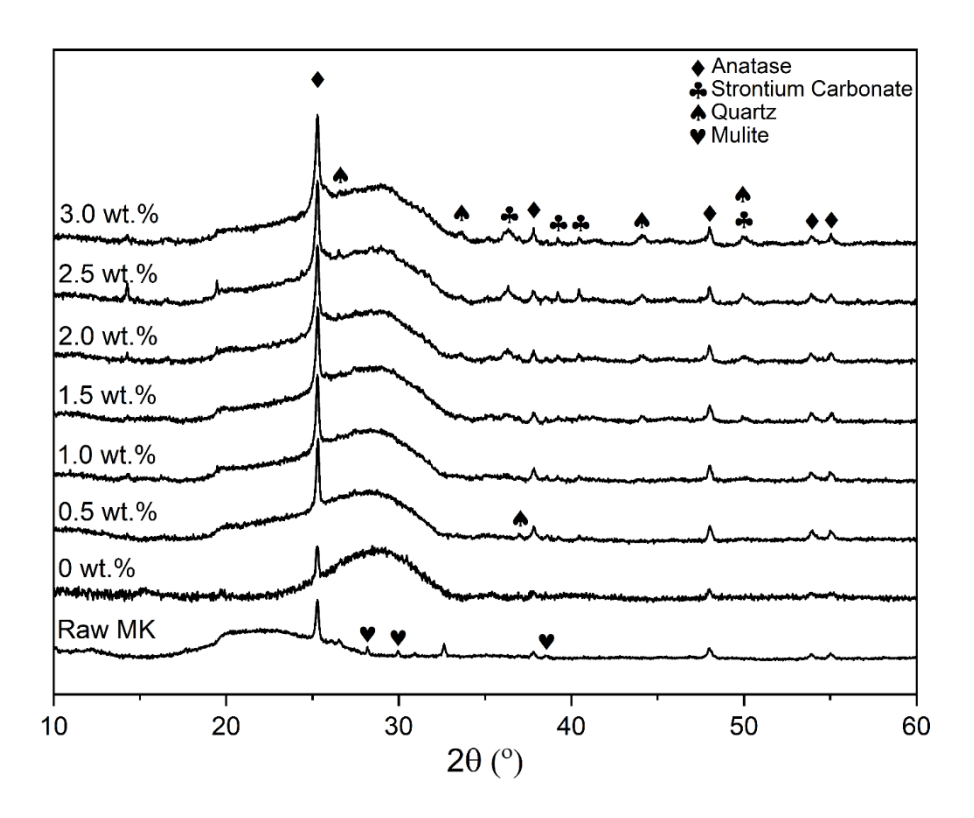


**Figure 1:** X-ray diffraction patterns of the reacted metakaolin-based geopolymers containing an incremental increase in the wt. % of Sr(OH)·8H<sub>2</sub>O within these samples.

#### 3.1.2 Fourier transform infrared spectroscopy

The FTIR spectrum for each of the samples produced to assess the effect of the Sr loading on the chemical immobilisation mechanism (Figure 2) exhibits bands consistent with common Si and Al bonding environments in an N–A–S–H gel [18], and a detailed analysis and discussion of these is provided in Supporting Information. A small band is observed approximately 1460 cm<sup>-1</sup> in the FTIR data for geopolymer gels produced with varying amounts of  $Sr(OH)_2 \cdot 8H_2O$ , and is assigned to asymmetric stretching vibrations of  $CO_3^{2-}$  anions in  $SrCO_3$  [35]. While this band is of low intensity, it is observed to at least some extent in all geopolymer gels containing Sr, and with intensity increasing steadily with increasing amounts of  $Sr(OH)_2 \cdot 8H_2O$  in the geopolymer formulation. This indicates formation of  $SrCO_3$  occurs when these geopolymer wasteforms contain 0.5 wt. %  $Sr(OH)_2 \cdot 8H_2O$ , due to reaction of atmospheric  $CO_2$  with excess  $Sr^{2+}_{(aq)}$  not incorporated into the N-A-S-H gel framework. The amount of  $SrCO_3$  formed increases with increasing amounts of  $Sr(OH)_2 \cdot 8H_2O$ . Formation of  $SrCO_3$  or  $CaCO_3$  was not observed in previous work investigating encapsulation of Sr and  $SrCO_3$  or  $SrCO_3$  or SrC

(0.5 mol.% of monovalent Na replaced by Sr, equivalent to 0.5 wt. % Sr(OH)<sub>2</sub>·8H<sub>2</sub>O in the geopolymer formulation).

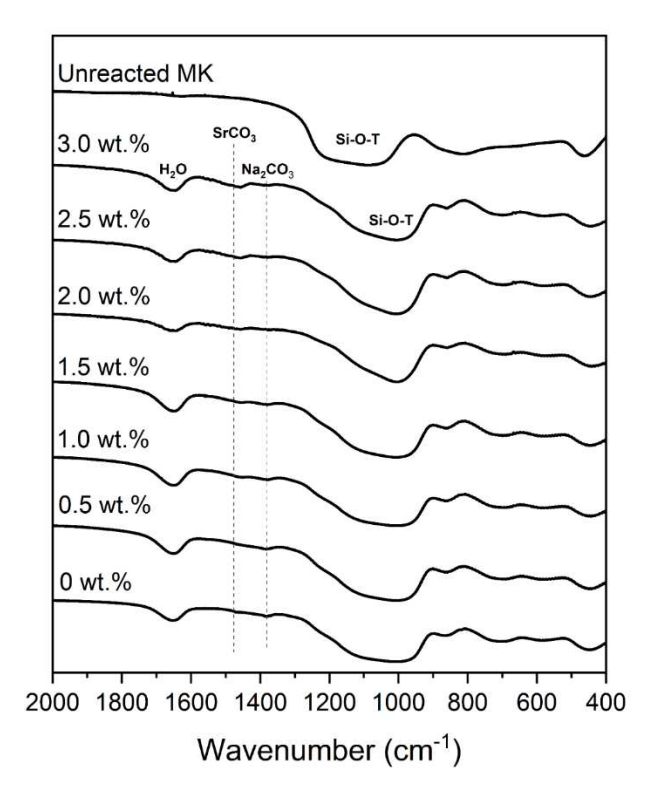


**Figure 2:** FTIR data for the geopolymers as a function of the amount of  $Sr(OH)_2 \cdot 8H_2O$  (wt. %) in the geopolymer formulation, and unreacted metakaolin,. Inset, the 1360 - 1560 cm<sup>-1</sup> range is highlighted to show the  $SrCO_3$  formation. Annotations are provided for bands attributed to asymmetric stretching vibrations of  $CO_3^2$  anions in  $SrCO_3$  and  $Na_2CO_3$ , bands due to free and chemically bound water, and bands due to asymmetric stretching of Si-O-T bonds (where T=AI or Si) in the N-A-S-H gel.

#### 3.1.3 Solid state nuclear magnetic resonance spectroscopy

# 3.1.3.1 <sup>29</sup>Si MAS and <sup>1</sup>H-<sup>29</sup>Si CP MAS NMR

The <sup>29</sup>Si MAS and <sup>1</sup>H-<sup>29</sup>Si CP MAS NMR data for the samples produced to assess the effect of the Sr loading on the chemical immobilisation mechanisms and Sr binding capacity of the N-A-S-H gel is shown in Figure 3. Each spectrum exhibits a broad resonance centred at  $\delta_{iso}$  = -87.0 ppm and spanning from  $\delta_{iso}$  = -75 to -110 ppm, with a consistent lineshape for all samples. This resonance is attributed to a distribution of Q<sup>4</sup>(mAl) environments (where  $0 \le m \le 4$ ) within a N-A-S-H gel, [36, 37] and the difference in the resonance

compared with that of metakaolin published previously [18, 38] indicates a reaction product comprising predominantly  $Q^4(4AI)$  and  $Q^4(3AI)$  sites.

The  $^{1}\text{H}^{-29}\text{Si}$  CP MAS NMR data for each geopolymer exhibits a broad resonance centred at  $\delta_{iso}$  = -84.0 ppm and spanning from  $\delta_{iso}$  = -75 to -95 ppm, with a consistent lineshape for all samples. Si sites in the hydrated N-A-S-H gel can be resolved from those in unreacted metakaolin by comparison of the  $^{1}\text{H}^{-29}\text{Si}$  CP MAS NMR data with the  $^{29}\text{Si}$  MAS NMR data. The maximum intensity at  $\delta_{iso}$  = -84.0 ppm in the  $^{1}\text{H}^{-29}\text{Si}$  CP MAS NMR spectra of the geopolymer gels, therefore, indicates that the N-A-S-H gel comprises primarily Q<sup>4</sup>(4Al) Si sites.

Deconvolution and quantification of the  $^{29}$ Si MAS and  $^{1}$ H- $^{29}$ Si CP MAS NMR data (Figure 3 and Table 6) identifies Q<sup>4</sup>(4AI), Q<sup>4</sup>(3AI) and Q<sup>4</sup>(2AI) sites within an Al-rich (Si/Al  $\leq$  1.2), fully polymerised (N,K)-A-S-H gel [17], resonating at  $\delta_{iso}$  = -83.4, -89.4 ppm and -95.0 ppm, respectively. Engelhardt's formula [39] (equation 1) can be used to calculate the molar Si/Al ratio of the N-A-S-H gel by assuming that there are negligible Al-O-Al bonds present (valid in geopolymers with Si/Al > 1 [40]).

291 
$$\frac{\text{Si}}{\text{Al}} = \frac{\sum_{m=1}^{4} I_{A_{Q^4(m\text{Al})}}}{\sum_{m=1}^{4} 0.25 \times m \times I_{A_{Q^4(m\text{Al})}}}$$

In equation 1,  $I_{AQ}^4$ <sub>(mAl)</sub> represents the normalised relative integral areas of each Q<sup>4</sup>(*m*Al) site within the N-A-S-H gel (i.e. excluding resonances due to Q<sup>4</sup>(*m*Al) sites within remnant unreacted metakaolin).

Each N-A-S-H gel exhibits a Si/Al value lower than that of the initial reaction mixtures (Si/Al = 1.19 to 1.22), indicating preferential release of Al during the dissolution of metakaolin, and subsequent formation of an Al-rich gel.

No consistent variation in the Si/Al ratio of the geopolymer gels is observed (within the estimated error) when comparing different amounts of added Sr(OH)<sub>2</sub>.8H<sub>2</sub>O, indicating that the incorporation of Sr (either by chemical immobilisation or physical encapsulation) in the geopolymers does not induce significant changes to the N-A-S-H gel structure. This contrasts with previous work investigating the incorporation of much smaller amounts of Sr in geopolymer cements (up to 0.012 wt. % Sr relative to the total sample mass and 0.026 mol % Sr relative to the total Na content) [18], which saw a slight decrease in the Si/Al ratio of the N-A-S-H gel with the incorporation of Sr<sup>2+</sup>. This is in line with replacement of a monovalent alkali cation with a divalent charge alkaline earth cation, resulting in an increased charge balancing

capacity. The differences observed in the samples here are likely due to the formation of SrCO<sub>3</sub> in the geopolymers investigated. The implications of this will be discussed in further detail below.

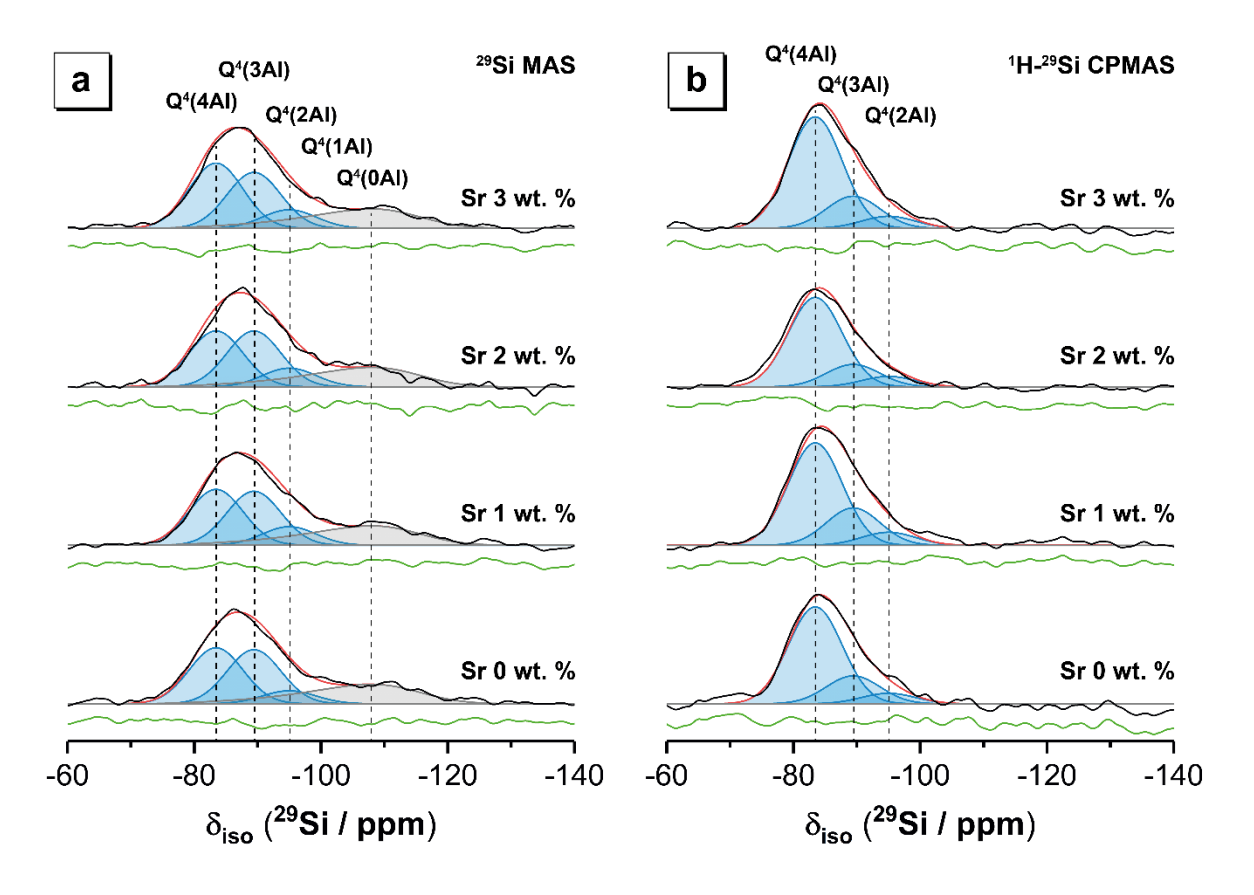


**Figure 3:** a) <sup>29</sup>Si MAS (B<sub>0</sub> = 11.7 T,  $v_R$  = 12.5 kHz) NMR and b) <sup>1</sup>H-<sup>29</sup>Si CP MAS (B<sub>0</sub> = 11.7 T,  $v_R$  = 12.5 kHz and Hartmann-Hahn contact period t = 1.7 ms) NMR spectra and associated deconvolutions for geopolymer gels, as a function of the amount of  $Sr(OH)_2 \cdot 8H_2O$  (wt. %) in the geopolymer formulation. The fit (shown in red) is the sum of the deconvoluted peaks, the data for each sample are shown in black, and the difference between the data and the fit is shown in green. Peaks attributed to Si sites in N-A-S-H are shown in blue, while peaks attributed to sites within unreacted metakaolin are shown shaded in grey.

**Table 6:** Relative integral areas for Q<sup>4</sup>(mAl) sites within N-A-S-H in each sample, calculated from the deconvoluted <sup>29</sup>Si MAS NMR spectra.

# Relative integral area (%)<sup>a</sup>

Sample O (wt. 9	Sr(OH)₂·8H₂ O (wt. %) in	Nominal	Q <sup>4</sup> (4AI)	Q <sup>4</sup> (3AI)	Q <sup>4</sup> (2AI)	Q4(1AI)	Q <sup>4</sup> (0AI)	Si/Al
	reaction mix	Sr/Na	$\delta_{iso}$ = -83.4	$\delta_{iso}$ = -89.4	$\delta_{iso}$ = -95	Q (IAI)	Q (UAI)	
A	0.0	0.000	45	44	11	0	0	1.19
С	1.0	0.009	43	42	14	0	0	1.22
E	2.0	0.018	43	43	14	0	0	1.22
G	3.0	0.027	47	40	13	0	0	1.20

<sup>&</sup>lt;sup>a</sup> The relative integrated intensity for each resonance is normalised to the sum of all sites within the reaction product and is obtained by simulating the <sup>29</sup>Si MAS NMR spectra. Residual unreacted metakaolin component contributions were observed in all geopolymer gel spectra and are shown in Figure 3 but are excluded from the quantification of N-A-S-H gel constituents. The estimated error in the relative integral area is 1 %. Peak full width at half maximum (FWHM) for all  $Q^4(mAl)$  environments is 10.0 ppm.

# 3.1.3.2 <sup>27</sup>AI MAS NMR

317

318

319

320

321

322

323

324

325326

327

328

329330

331332

333

334

<sup>27</sup>Al MAS NMR data for the samples produced to assess the effect of the Sr loading on the chemical immobilisation mechanism are shown in Figure 4. Each spectrum exhibits a broad resonance centred at  $\delta_{\text{obs}} = 60.7$  ppm and spanning from  $\delta_{\text{obs}} = 70$  to 50 ppm, which indicates AI within a tetrahedral (q<sup>4</sup>) site in a (N,K)-A-S-H type gel [40, 41], with the negative charge due to Al3+ in tetrahedral coordination balanced by alkali cations (Na<sup>+</sup> or K<sup>+</sup>). A relatively low intensity resonance, spanning from  $\delta_{obs}$  = 10 to 0 ppm and centred at  $\delta_{obs}$  = 6 ppm, is also observed in the <sup>27</sup>Al MAS NMR spectrum for each geopolymer gel and is attributed to Al in octahedral coordination (AlO<sub>6</sub> sites) in unreacted metakaolin particles [41, 42]. The <sup>27</sup>Al MAS NMR spectrum for unreacted metakaolin has been published previously and displays three broad resonances due to Al in tetrahedral, pentahedral, and octahedral coordination exhibiting distributions of  $\delta_{obs}$  with maximum intensity at  $\delta_{obs}$  = 56, 33 and 8 ppm, respectively [18, 41, 42]. The presence of Al in predominantly tetrahedral coordination in the <sup>27</sup>Al MAS NMR spectrum for each geopolymer gel (Figure 4) in the study presented here is expected due to the presence of excess alkali cations [43]. This indicates that most of the Al within metakaolin has reacted and is in line with the <sup>29</sup>Si MAS and <sup>1</sup>H-<sup>29</sup>Si CP MAS NMR observations above. Similar to previous observations for geopolymer cements incorporating up to 0.012 wt. % Sr (relative to the total sample mass) and 0.026 mol % Sr (relative to the total Na content) [18], the width and lineshape of the distributions of  $\delta_{obs}$  in the <sup>27</sup>Al MAS NMR data for each geopolymer investigated

here are identical, indicating that incorporation of Sr<sup>2+</sup> cations in the N-A-S-H gel does not alter the local structure of the aluminosilicate framework such that it is observable by NMR.

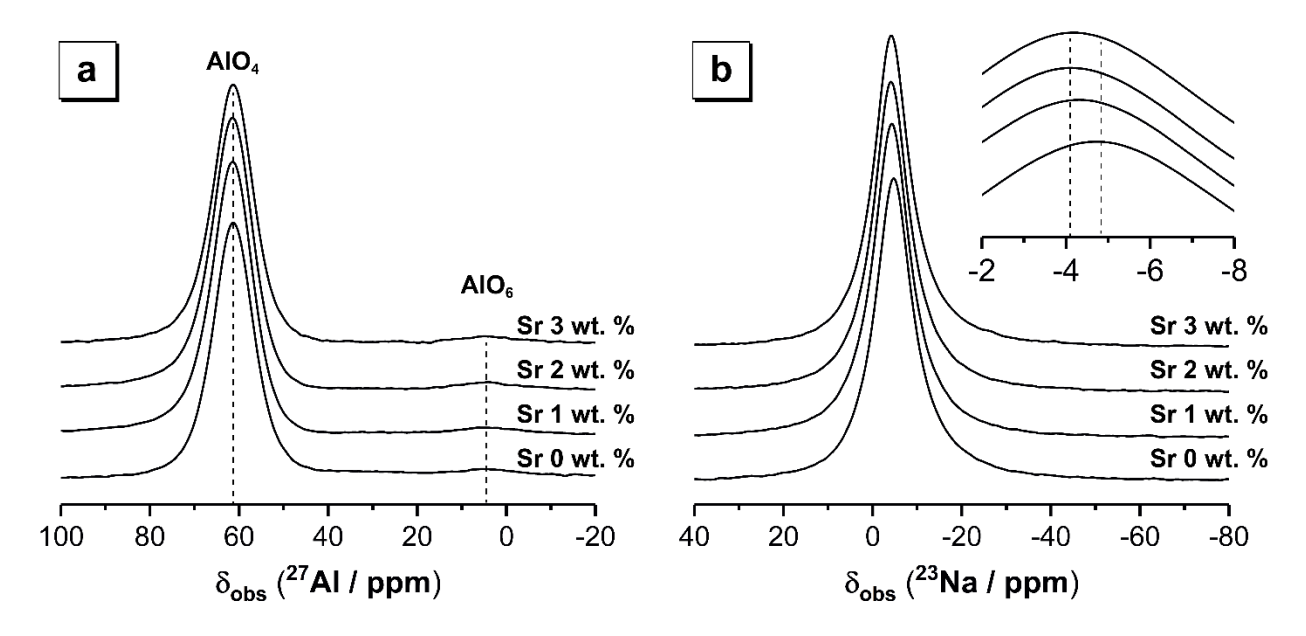


**Figure 4:** a) <sup>27</sup>Al MAS NMR spectra ( $B_0 = 11.7 \text{ T}$ ,  $v_R = 12.5 \text{ kHz}$ ) and b) <sup>23</sup>Na MAS NMR spectra ( $B_0 = 11.7 \text{ T}$ ,  $v_R = 12.5 \text{ kHz}$ ) for each geopolymer gel. The inset in b) shows a magnified region of the <sup>23</sup>Na MAS NMR spectra.

# 3.1.3.3 <sup>23</sup>Na MAS NMR

The  $^{23}$ Na MAS NMR spectrum for the samples produced to assess the effect of the Sr loading on the chemical immobilisation mechanism is shown in Figure 4. Each spectrum exhibits a broad resonance spanning from  $\delta_{obs}$  = 10 to -20 ppm, attributed to Na<sup>+</sup> ions charge balancing Al<sup>3+</sup> ions in fully polymerised q<sup>4</sup> sites within the N-A-S-H gel [37, 40, 41]. In the absence of Sr (i.e. the 0.0 wt. % Sr sample), the  $^{23}$ Na MAS NMR spectrum of the geopolymer gel has a maximum intensity at  $\delta_{obs}$  = -5.0 ppm. Incorporation of Sr<sup>2+</sup> shifts this  $^{23}$ Na resonance toward higher  $\delta_{obs}$  values (see inset of Figure 4b), exhibiting a maximum at  $\delta_{obs}$  = -4.0 ppm in geopolymer gels with  $\geq$  1.0 wt. % Sr(OH)<sub>2</sub>.8H<sub>2</sub>O. This indicates decreased shielding of Na<sup>+</sup>, contrasting with previous observations for significantly lower Sr-loadings (up to 0.012 wt. % Sr, relative to the total sample mass) [18]. In that study, incorporation of up to 0.012 wt. % Sr resulted in increased shielding of Na<sup>+</sup> in the  $^{23}$ Na MAS NMR data, consistent with the displacement of Na<sup>+</sup> with Sr<sup>2+</sup>, which was expected to fulfil an equivalent charge balancing role. The  $^{23}$ Na MAS NMR data presented here suggest that in geopolymers containing  $\geq$  1.0 wt. % Sr(OH)<sub>2</sub>.8H<sub>2</sub>O, the formation of SrCO<sub>3</sub> and Na<sub>2</sub>CO<sub>3</sub> (observed

via XRD and FTIR, and discussed above in sections 2.1.2.1 and 2.1.2.2, respectively) reduces the amount of  $Sr^{2+}$  incorporated into the N-A-S-H gel. This is consistent with the absence of any observable variation in the distribution of  $\delta_{obs}$  in the  $^{27}$ Al MAS,  $^{29}$ Si MAS and  $^{1}$ H- $^{29}$ Si CP MAS NMR data for the geopolymer gels presented here. If significant quantities of Sr were incorporated in the N-A-S-H gel structure, substitution of the divalent alkali earth cations ( $Sr^{2+}$ , Shannon ionic radii = 1.18 Å for octahedrally coordinated  $Sr^{2+}$ ) for twice the amount of single valence alkali cations ( $Na^{+}$ , Shannon ionic radii 1.02 Å for octahedrally coordinated  $Na^{+}$ ) would be expected to distort the local structure of the (N,N)-A-S-H gel framework. It is likely that both thermodynamic and kinetic factors influence the incorporation of Sr into the N-A-S-H gel here. At high pH, as occurs in fresh geopolymer pastes,  $SrCO_3$  exhibits very low solubility and hence strong stability, and so once formed this phase can be considered stable. Kinetic and steric hindrance will also impede incorporation of any soluble Sr into the alkali aluminosilicate gel once the gel begins to precipitate from solution.

Together with the XRD and FTIR data discussed above, this suggests that the limit for chemical immobilisation of  $Sr^{2+}$  in geopolymer gels via incorporation into the N-A-S-H gel framework is equal to or below Sr/Na = 0.005 (0.5 mol.% of monovalent Na replaced by divalent Sr, equivalent to 0.5 wt. %  $Sr(OH)_2 \cdot 8H_2O$  in the geopolymer formulation). While the geopolymers appear to encapsulate Sr as  $SrCO_3$  at these higher waste loadings, the findings here of the limit of chemical immobilisation of Sr have significant implications for the solidification of Sr-bearing wastes in geopolymers.

# 3.1.4 X-ray absorption spectroscopy

# 3.1.4.1 Sodium silicate-activated samples

#### 3.1.4.1.1 X-ray absorption near-edge structure (XANES) spectroscopy

Normalised Sr K-edge X-ray absorption spectra for the samples produced to assess the effect of the Sr loading on the chemical immobilisation mechanisms and Sr binding capacity of the N-A-S-H gel are shown in Figure 5 (samples Sr 0.014 wt.%, Sr 1 wt.%, Sr 2 wt.%, Sr 3 wt.%, with Sr/Al = 0.00025, 0.018, 0.035, and 0.053, respectively). Data from standard compounds of SrCO<sub>3</sub> [44] and the mineral brewsterite-Sr,  $(Sr,Ba)_2Al_4Si_{12}O_{32}\cdot10H_2O$ , [45] are overlaid for comparison.

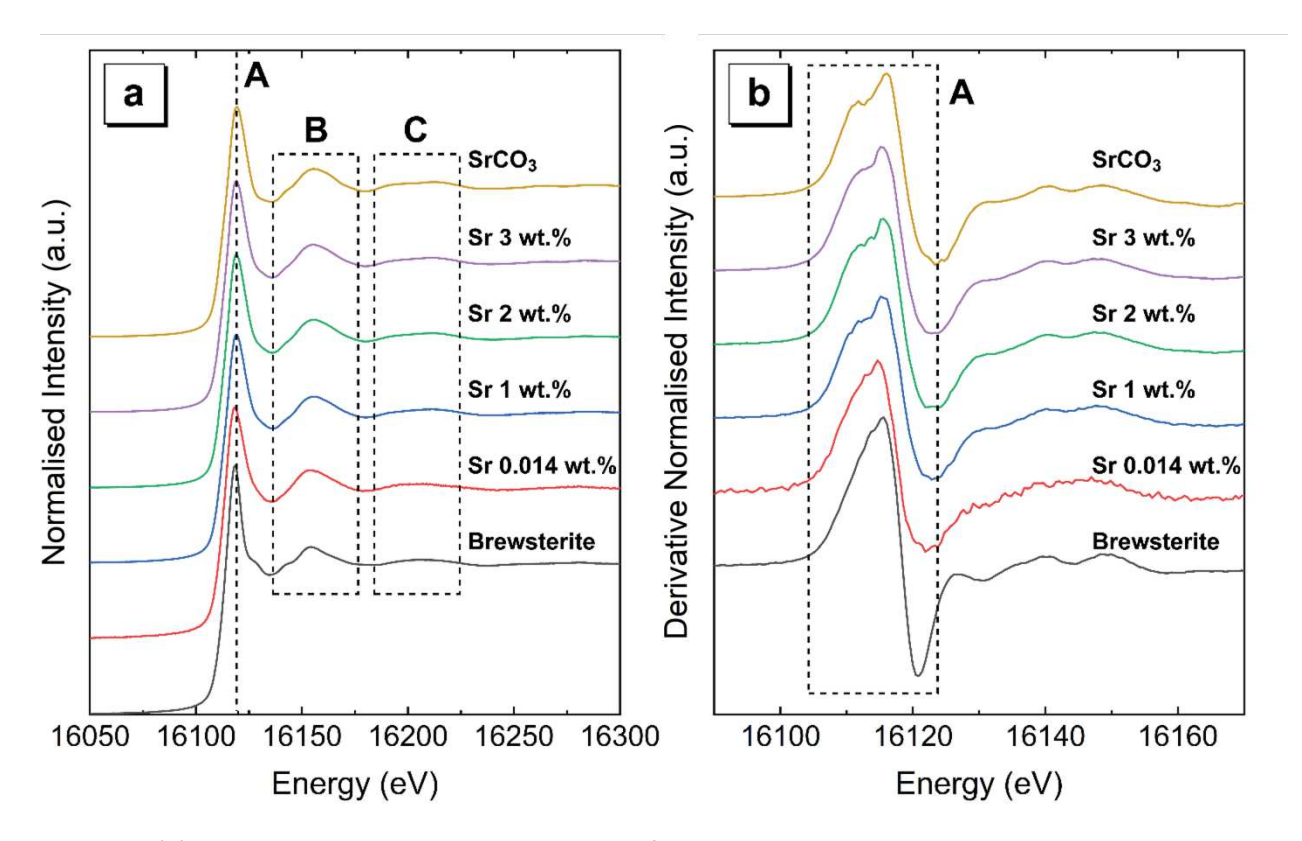


**Figure 5:** (a) Normalised X-ray absorption spectra for the Sr-doped geopolymers samples. Overlaid are data from the mineral brewsterite-Sr and SrCO<sub>3</sub>. (b) 1st derivative of the spectra. The spectra have been stacked to improve clarity.

The Sr K-edge is characterised by a smoothly rising absorption edge with a single peak at the maximum. Although the absorption edge is relatively featureless (cf. K-edge spectra of transition metals [46-49]) there are several groups of features, ca. 35 eV and 85 eV above the peak of the absorption edge, which can be used as qualitative diagnostic tools. Close inspection of the absorption edge Figure 5(a) reveals a small shift in the position of the maximum to lower energy in the brewsterite-Sr mineral with respect to the SrCO<sub>3</sub>. The dotted line labelled A is included as a guide to the eye. A shallow shoulder on the leading edge of the peak is barely perceptible; however, on inspection of the 1st derivative Figure 5(b) this feature is clearly evidenced by the presence of two components on the feature labelled A (Feature A) inside the hatched box. The relative intensity and position of the two components of the doublet are different in the two standard compounds; the lower energy component in the brewsterite-Sr is reduced to a shallow shoulder on the leading energy edge. Direct comparison between the spectra from the samples loaded with  $\geq 1$  wt. % Sr(OH)<sub>2</sub>·8H<sub>2</sub>O, and the standards indicate that the local environment of Sr in these samples is structurally similar to that found in SrCO<sub>3</sub>. The edge position for the spectrum from the sample loaded with 0.014 wt. % Sr(OH)<sub>2</sub>·8H<sub>2</sub>O (molar Sr/Al = 0.00025) and the features in the 1st derivative are more

characteristic of Sr in a zeolitic structural environment (e.g. brewsterite-Sr). Inspection of the spectral features above the absorption edge (indicated by the hatched regions labelled B and C in Figure 5(a) also show similarities between the spectra for the geopolymers loaded with higher amounts of Sr and that for SrCO<sub>3</sub>. The broad and diffuse nature of these features in the Sr 0.014 wt. % loaded sample indicates that the local structural environment in this sample is relatively disordered (beyond the first nearest neighbour anion coordination sphere) in comparison to that of the brewsterite-Sr. These conclusions corroborate the findings from the XRD analysis (Figure 1).

# 

# 3.1.4.1.2 Extended X-ray Absorption Fine Structure (EXAFS)

Figure 6(a) shows the extracted EXAFS region of the spectra (in wavenumber space).



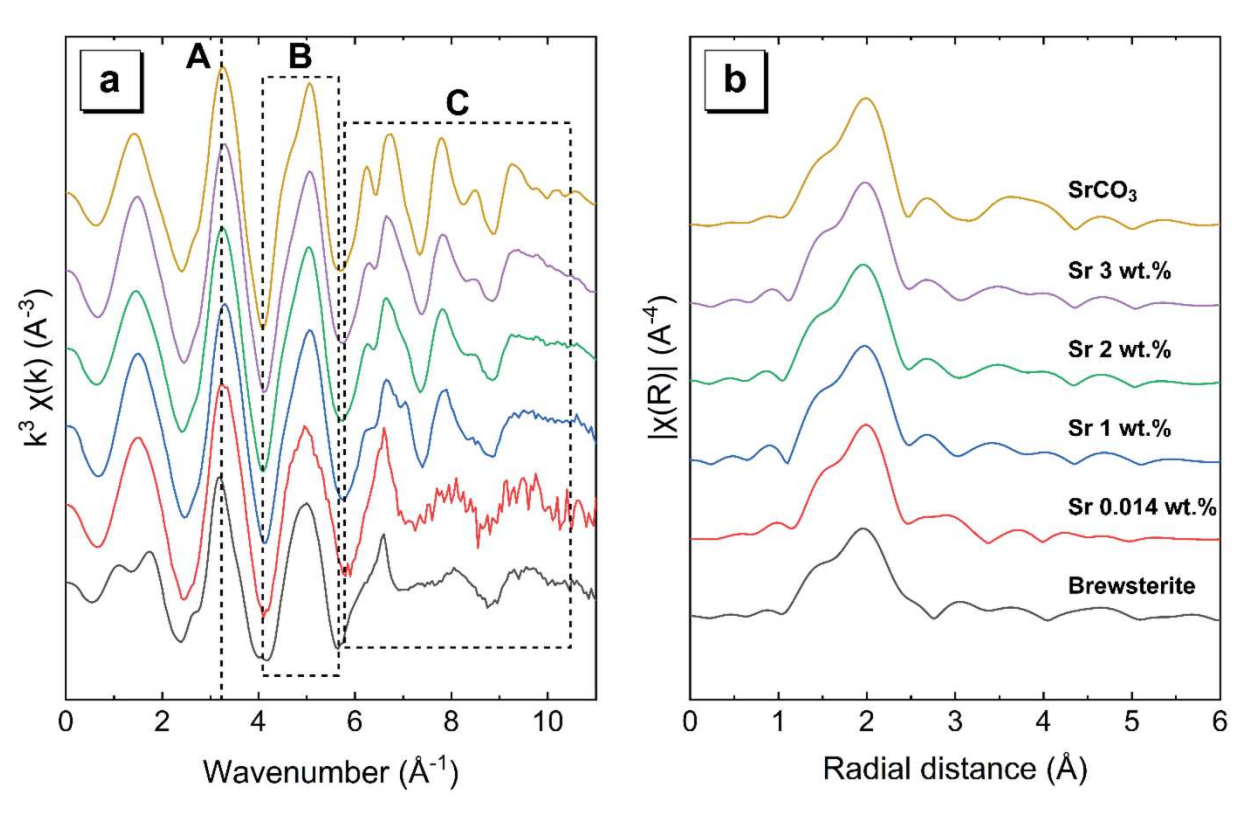


**Figure 6:** (a)  $k^2$ -weighted X(k) and (b) the Fourier transforms (FT) of  $k^2$ -weighted X(k) for the Sr-doped geopolymer and standard samples. The spectra have been stacked to improve clarity.

To accurately determine a first shell coordination number ( $N_0$ ), an independent determination of the amplitude reduction factor ( $S_0^2$ ) is required [50, 51]. It is not possible to simultaneously refine both.  $S_0^2$ 

was therefore determined by fitting the structural model reported by Pannhorst and Lohn [44] to the SrCO<sub>3</sub> data set. The model consists of a nearest neighbour oxygen anion shell, with a degeneracy of nine, and two farther out cation shells with refined scattering path lengths of  $3.37 \pm 0.10$  Å (Sr-C) and  $4.17 \pm 0.02$  Å (Sr-Sr). The degeneracy of both these shells was six, and their inclusion allowed a satisfactory fit for the features in the FT between 3 and 5 Å. Validation of the proposed chemical structure was performed using the bond valence method [52], and further details are provided in Supporting Information. The refined model parameters are reported in Table S1, Supporting Information. The refined Sr-O scattering path length was  $2.63 \pm 0.03$  Å, and the bond valence sum (BVS) returned a value of  $2.2 \pm 0.1$  v.u., which is within 10% of the formal Sr valence value of 2. Bond valence parameters were taken from Gagné and Hawthorne [53]. The  $k^3$  weighted X(k) and FT, together with the fits to the structural model, are shown in Figure 7.



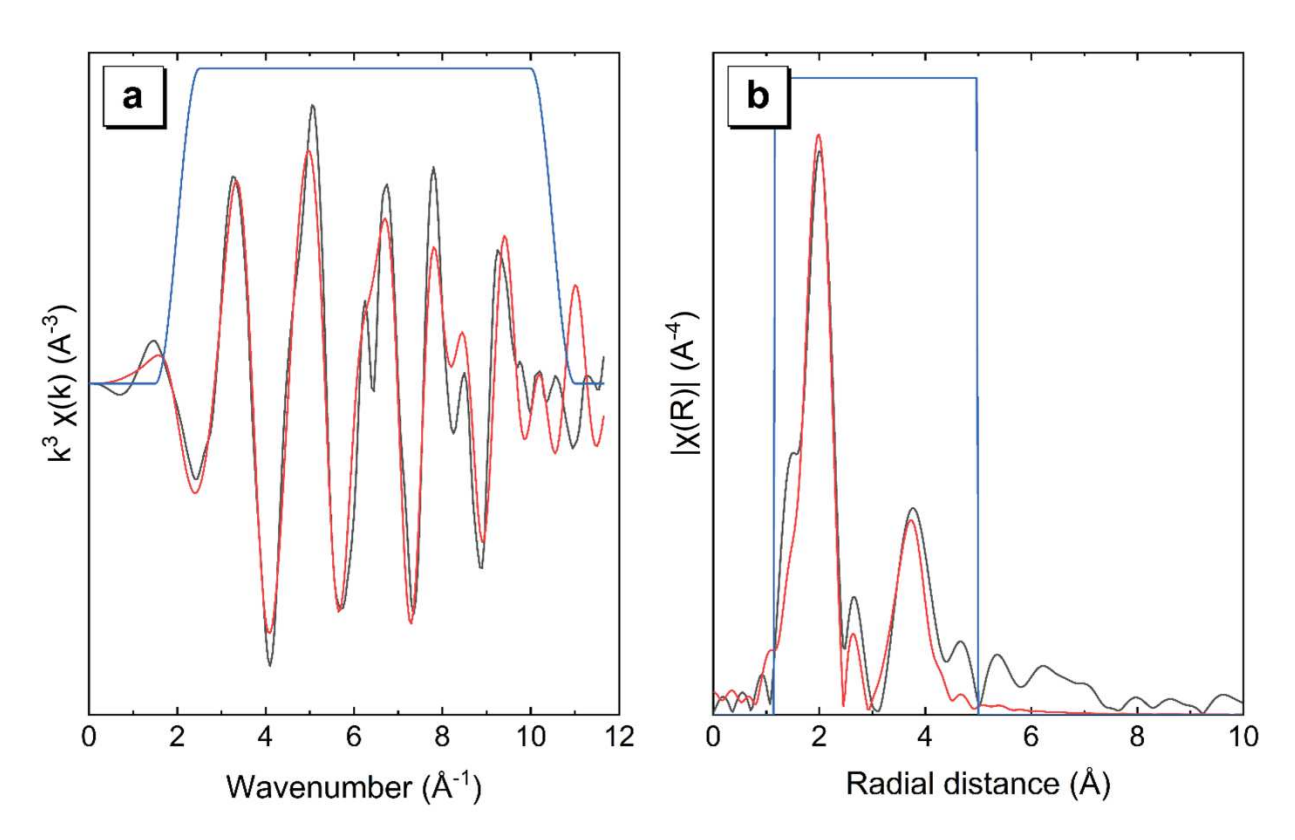


Figure 7:  $k^3\chi(k)$  and FT of  $k^3\chi(k)$  for SrCO<sub>3</sub> (uncorrected for phase shift). Solid black lines represent experimental data, and solid red lines represent theoretical fits. Fitting windows are indicated by solid blue lines.

In light of the qualitative similarities observed with respect to SrCO<sub>3</sub>, the Sr K-edge EXAFS data for geopolymer samples loaded with ≥ 1 wt. % Sr(OH)<sub>2</sub>·8H<sub>2</sub>O (molar Sr/Al = 0.018, 0.035, and 0.053 for samples labelled Sr 1.0, Sr 2.0, and Sr 3.0 wt. %, respectively) were modelled using the same basic structural model. The amplitude reduction factor (S<sub>0</sub><sup>2</sup>) was fixed, based on the refinement of the SrCO<sub>3</sub> data, at 0.8 ± 0.2 and the first shell (Sr-O) coordination number was allowed to refine. The degeneracies for the second (Sr-C) and third (Sr-Sr) nearest neighbour shells were initially fixed according to the SrCO<sub>3</sub> structural model outlined above. A single Sr-Sr coordination shell did not provide a satisfactory fit to the spectral features in the  $k^3$ -weighted X(k) between 3 and 5 Å so the six Sr atoms were split into two groups of three. The inclusion of two Sr-Sr paths with a scattering length at ca. 4 Å, and a degeneracy of three, provided sufficient flexibility in the model to return a satisfactory fit. The refined model parameters are reported in Table S2, Supporting Information. Very similar fits were returned for the geopolymer samples loaded with 1.0, 2.0, and 3.0 wt. % Sr(OH)<sub>2</sub>·8H<sub>2</sub>O, indicating that the predominant Sr environment in these samples was similar to that in SrCO<sub>3</sub>. The refined Sr-O scattering path length (2.58 ± 0.01 Å) were consistent with the slightly lower refined Sr-O shell coordination numbers, which varied between 7.6 ± 0.6 and 7.9 ± 0.7. The BVS sum calculations were all within 5 % of the formal Sr valence value, which indicates that the refined path lengths were sensible given the number of nearest neighbour anions in the first coordination shell. Qualitative inspection of the data obtained for the sample loaded with 0.014 wt. % Sr(OH)<sub>2</sub>·8H<sub>2</sub>O (molar Sr/Al = 0.00025) showed similarities with data from the brewsterite-Sr standard. This indicated that the Sr local environment at low dopant concentration is better represented using a model based on a zeolitelike structure. A model was constructed based on the structural refinement reported by Artioli et al. [45], which consisted of: a nearest neighbour Sr-O shell with a refined path length of 2.68 ± 0.03 Å; Sr-Si shells at ca. 3.5, 5.6, and 7.0 Å; Sr-Al shells at ca. 3.9, 5.5, and 6.5 Å; five Sr-O shells with path lengths between ca. 4.3 and 6.4 Å; a single Sr-Sr shell at ca. 6.9 Å. The refined parameters are reported in full, in Table S3, Supporting Information. As in previous models, the BVS was used as a restraint, returning a value of 2.2 ± 0.1 v.u. The refined coordination number for the Sr-O shell was 10.0 ± 1.2, which was consistent with the proposed starting model [45]. A simplified version of this model was applied to the data for the sample loaded with 0.014 wt. % Sr(OH)<sub>2</sub>·8H<sub>2</sub>O (molar Sr/Al = 0.00025), which consisted of a nearest neighbour Sr-O shell (2.68 ± 0.03 Å) and two Sr-cation shells (Sr- Si and Sr-Al). The coordination numbers for the Sr-Si and Sr-Al shells were fixed, and a Si/Al ratio of 1.33 was maintained to be consistent with the nominal chemical composition of the reaction mixtures (see Table 2 and Table 3). The refined Sr-O coordination number was 9.3 ± 0.8, which is consistent with the Sr atoms adopting structural positions within the

432

433 434

435

436

437

438

439

440 441

442

443

444

445

446

447

448

449

450

451

452

453

454

455 456

457

458

459

460

461

462

cavities in a pseudo-zeolitic framework structure similar to that of brewsterite-Sr. The BVS restraint returned a value of  $2.0 \pm 0.1$  v.u. In order to rule out strontium accommodation in the sodium positions in the N-A-S-H framework structure [40, 54] the Sr-O coordination number was fixed at six to determine whether a fit to SrCO<sub>3</sub> could be achieved. This was unsuccessful, indicating that Sr is present in a pseudo-zeolitic framework.

Together with the XRD, FTIR and SSNMR data discussed above, this confirms that the limit for chemical immobilisation of  $Sr^{2+}$  in these geopolymer gels via incorporation into the pseudo-zeolitic N-A-S-H gel framework is equal to or below Sr/Na = 0.005 (0.5 mol.% of monovalent Na replaced by divalent Sr, equivalent to 0.5 wt. %  $Sr(OH)_2 \cdot 8H_2O$  in the geopolymer formulation). Above this amount, any additional Sr exists in a phase exhibiting structural similarity with  $SrCO_3$ .

### 3.2 Effect of the alkali cation on the chemical immobilisation mechanism

# 3.2.1 Solid state nuclear magnetic resonance spectroscopy

# 3.2.1.1 <sup>29</sup>Si MAS and <sup>1</sup>H-<sup>29</sup>Si CP MAS NMR

A detailed discussion of the <sup>29</sup>Si MAS and <sup>1</sup>H-<sup>29</sup>Si CP MAS NMR data for samples produced to assess the effect of the alkali cation on the chemical immobilisation mechanism has been published previously [18]. This data is also presented in Figure S1, Supporting Information, aid interpretation of the <sup>27</sup>Al MAS and <sup>39</sup>K MAS NMR data, presented here and discussed in the remainder of this paper. Quantification of the <sup>29</sup>Si MAS NMR deconvolutions for each geopolymer shows that incorporation of Ca<sup>2+</sup> and Sr<sup>2+</sup> results in a slight decrease in the Si/Al ratio of the (N,K)-A-S-H gel [18], consistent with substitution of a divalent charge alkaline earth cation for a monovalent alkali cation resulting in an increased charge balancing capacity within the gel framework [18]. Incorporation of both Ca<sup>2+</sup> and Sr<sup>2+</sup> did not result in any observable variation in gel Si/Al ratios (within the estimated error). This indicates that both Ca<sup>2+</sup> and Sr<sup>2+</sup> induce similar structural changes [18].

# 3.2.1.2 <sup>27</sup>Al MAS and 3QMAS NMR

The <sup>27</sup>Al MAS NMR data (Figure 8a) acquired at high field (20.0 T) for each geopolymer gel exhibit a broad tetrahedral Al resonance centred at  $\delta$  = 60.7 ppm and spanning from  $\delta$  = 70 to 50 ppm, indicating tetrahedral Al a (N,K)-A-S-H-type gel [40, 41], with the negative charge due to Al<sup>3+</sup> in tetrahedral coordination balanced by alkali cations (Na<sup>+</sup> or K<sup>+</sup>). With the exception of a narrowing of the distribution of chemical shifts, the data obtained at 20.0 T do not differ significantly from data obtained in this study at 14.1 and 9.4 T, and obtained previously at 11.7 T [18].

The excess alkali cations within the samples [43] means that observation of Al in only tetrahedral coordination is expected and indicates complete reaction of Al within metakaolin. This is consistent with the  $^{29}$ Si MAS and  $^{1}$ H- $^{29}$ Si CP MAS NMR data that shows preferential Al dissolution during reaction. The width and lineshape of this resonance are identical for each sample, regardless the different alkali (Na<sup>+</sup> or K<sup>+</sup>) or alkaline earth (Ca<sup>2+</sup>, Sr<sup>2+</sup>) cations present. When K<sup>+</sup> is present the  $^{27}$ Al nuclei are slightly shielded for geopolymers activated with Na<sub>2</sub>SiO<sub>3</sub> (in  $\delta$  = 60.9 ppm) compared with those activated with Na<sub>2</sub>SiO<sub>3</sub> or blended Na<sub>2</sub>SiO<sub>3</sub> and K<sub>2</sub>SiO<sub>3</sub> ( $\delta$  = 60.6 ppm), consistent with replacement of some of the charge balancing Na<sup>+</sup> ions with K<sup>+</sup> ions. The addition of Sr<sup>2+</sup> and Ca<sup>2+</sup> results in a slight narrowing of the chemical shift

distribution and an increase in intensity (between 1 and 3%) of the distribution maximum for all samples. This is consistent with the reduction in the Al/Si ratio observed by <sup>29</sup>Si MAS NMR discussed above.

<sup>27</sup>Al 3QMAS data (Figure 8b) were acquired to determine if incorporation of Sr<sup>2+</sup> and Ca<sup>2+</sup> resulted in changes in the symmetry around each Al nucleus within the geopolymer gels. The sheared <sup>27</sup>Al 3QMAS spectra for geopolymer cements produced from the reaction of metakaolin with potassium silicate each display a single Al<sup>IV</sup> resonance which is broadened primarily along the chemical shift (CS) axis. Each resonance indicates a single Al<sup>IV</sup> site linked via oxygen bridges to tetrahedral Si (i.e., Si<sup>IV</sup>–O<sup>-</sup>–Al<sup>IV</sup>), consistent with Si<sup>IV</sup>–O<sup>-</sup>–Al<sup>IV</sup> sites charge-balanced by Na<sup>+</sup> or K<sup>+</sup>. The absence of any variation in the <sup>27</sup>Al 3QMAS spectra for samples containing Sr and Ca, and the sample without, indicates incorporation of these cations does not result in changes to the local structure of Al in the (N,K)-A-S-H gel.

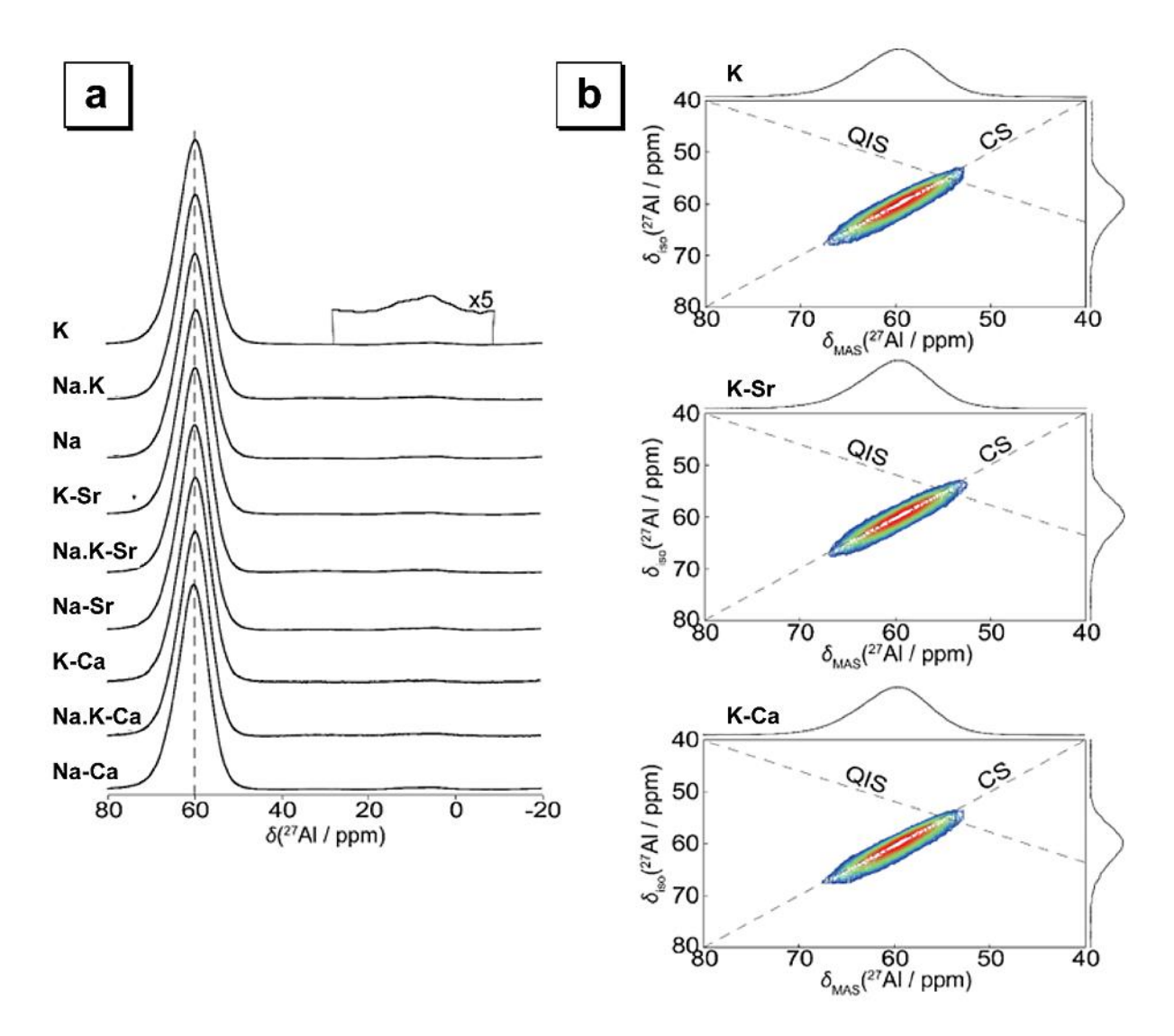


**Figure 8:** a)  $^{27}$ Al MAS NMR spectra (B<sub>0</sub> = 20.0 T,  $v_R$  = 20 kHz) for each geopolymer gel, and b)  $^{27}$ Al 3QMAS z-filter NMR spectra (B<sub>0</sub> = 20.0 T,  $v_R$  = 20 kHz) for each potassium silicate-activated geopolymer gel. Spectra are sheared, and the single pulse MAS NMR spectra is shown on the horizontal axis for comparison (F2 dimension). The chemical shift (CS) and quadrupolar induced shift (QIS) axes are indicated by the dashed lines.

# 3.2.1.3 <sup>23</sup>Na and <sup>39</sup>K MAS NMR

The  $^{23}$ Na MAS NMR data for the samples produced to assess the effect of the alkali cation on the chemical immobilisation mechanism has been published previously [18]; however, these data are presented here (Figure 9) to aid interpretation of the  $^{39}$ K MAS NMR data discussed in this section. The  $^{23}$ Na MAS NMR spectrum for each geopolymer gel (Figure 9) exhibits a broad resonance spanning from  $\delta$  = 10 to -20 ppm. This resonance is centred at  $\delta$  = -2.5 ppm for geopolymer gels activated with Na<sub>2</sub>SiO<sub>3</sub> or blended Na<sub>2</sub>SiO<sub>3</sub> and K<sub>2</sub>SiO<sub>3</sub>, and in these samples this resonance is attributed to charge balancing Na<sup>+</sup> ions within a (N,K)-A-S-H type gel [37, 40, 41]. The width and lineshape of the chemical shift distribution is very similar for geopolymers activated with Na<sub>2</sub>SiO<sub>3</sub> or with a combination of Na<sub>2</sub>SiO<sub>3</sub> and K<sub>2</sub>SiO<sub>3</sub>, suggesting that some of the charge balancing Na<sup>+</sup> ions are replaced by K<sup>+</sup> ions.

Incorporation of alkaline earth cations in the geopolymer results movement of the  $^{23}$ Na distribution of chemical shifts toward lower  $\delta$  values (see inset of Figure 9) after, and is centred at  $\delta$  = -3.2 ppm in geopolymers activated with Na<sub>2</sub>SiO<sub>3</sub> and  $\delta$  = -3.6 ppm in geopolymer gels activated with blended Na<sub>2</sub>SiO<sub>3</sub> and K<sub>2</sub>SiO<sub>3</sub>. This is consistent with Sr<sup>2+</sup> or Ca<sup>2+</sup> ions substitution for Na<sup>+</sup> ions, which then are expected to take on an equivalent charge balancing role. Substitution of one double valence alkali earth cation (i.e. Sr<sup>2+</sup> or Ca<sup>2+</sup>) for two single valence alkali cations is expected to perturb the (N,K)-A-S-H gel nanostructure, due to differences in charge and ionic size (Shannon ionic radii 1.02, 1.38, 1.00, and 1.18 Å for octahedrally coordinated Na<sup>+</sup>, K<sup>+</sup>, Ca<sup>2+</sup> and Sr<sup>2+</sup>, respectively).

Incorporation of  $Sr^{2+}$  or  $Ca^{2+}$  does not result in observable variation in the distribution of  $\delta$  in geopolymer gels, regardless of the alkali source. This indicates that at the concentrations investigated here the N,K)-A-S-H gel framework can easily accommodate both  $Sr^{2+}$  and  $Ca^{2+}$ , which is likely a result of their lack of long range order [40].

The  $^{39}$ K MAS NMR data (Figure 9) for each sample exhibits a broad resonance spanning from  $\delta$  = -20 ppm to -220 ppm, centred at  $\delta$  = -100 ppm. This indicates charge-balancing extra-framework K<sup>+</sup> ions within a (N,K)-A-S-H-type gel [55]. Similar to what was observed for the  $^{23}$ Na MAS NMR data, the width and lineshape of the chemical shift distribution in the  $^{39}$ K MAS NMR data is very similar for geopolymer gels activated with  $K_2SiO_3$  or with blended  $K_2SiO_3$  and  $Na_2SiO_3$ . This suggests that there is sufficient distance between charge balancing Na<sup>+</sup> and K<sup>+</sup> ions, and that there is no Na<sup>+</sup> present in the immediate local region surrounding K<sup>+</sup> ions.

In contrast to the trend observed in the  $^{23}$ Na MAS NMR data, no change in the lineshape or position of the  $^{39}$ K resonance is observed after incorporation of alkaline earth cations (see inset of Figure 9), in all geopolymer cements activated with either  $K_2SiO_3$  or blended  $Na_2SiO_3$  and  $K_2SiO_3$ . This indicates there are no observable changes in shielding of  $K^+$  after incorporation of  $Sr^{2+}$  or  $Ca^{2+}$  ions, suggesting that  $K^+$  ions are not displaced by  $Sr^{2+}$  or  $Ca^{2+}$  ions. This contrasts with observations from the  $^{23}$ Na MAS NMR data, discussed above, that indicated displacement of  $Na^+$  by  $Sr^{2+}$  or  $Ca^{2+}$  ions, which are then expected to provide an equivalent charge balancing role. However, synchrotron-based X-ray absorption data (discussed below) shows clear evidence of Sr within these geopolymer samples being in sites that are structurally similar to brewsterite at the lower Sr loading (0.014 wt. %). It is therefore likely that any changes in local structure of K caused by the displacement of  $K^+$  ions with  $Sr^{2+}$  are not observable by  $^{39}K$  MAS as a result of the broad lineshapes of the  $^{39}K$  MAS NMR resonances for these samples.

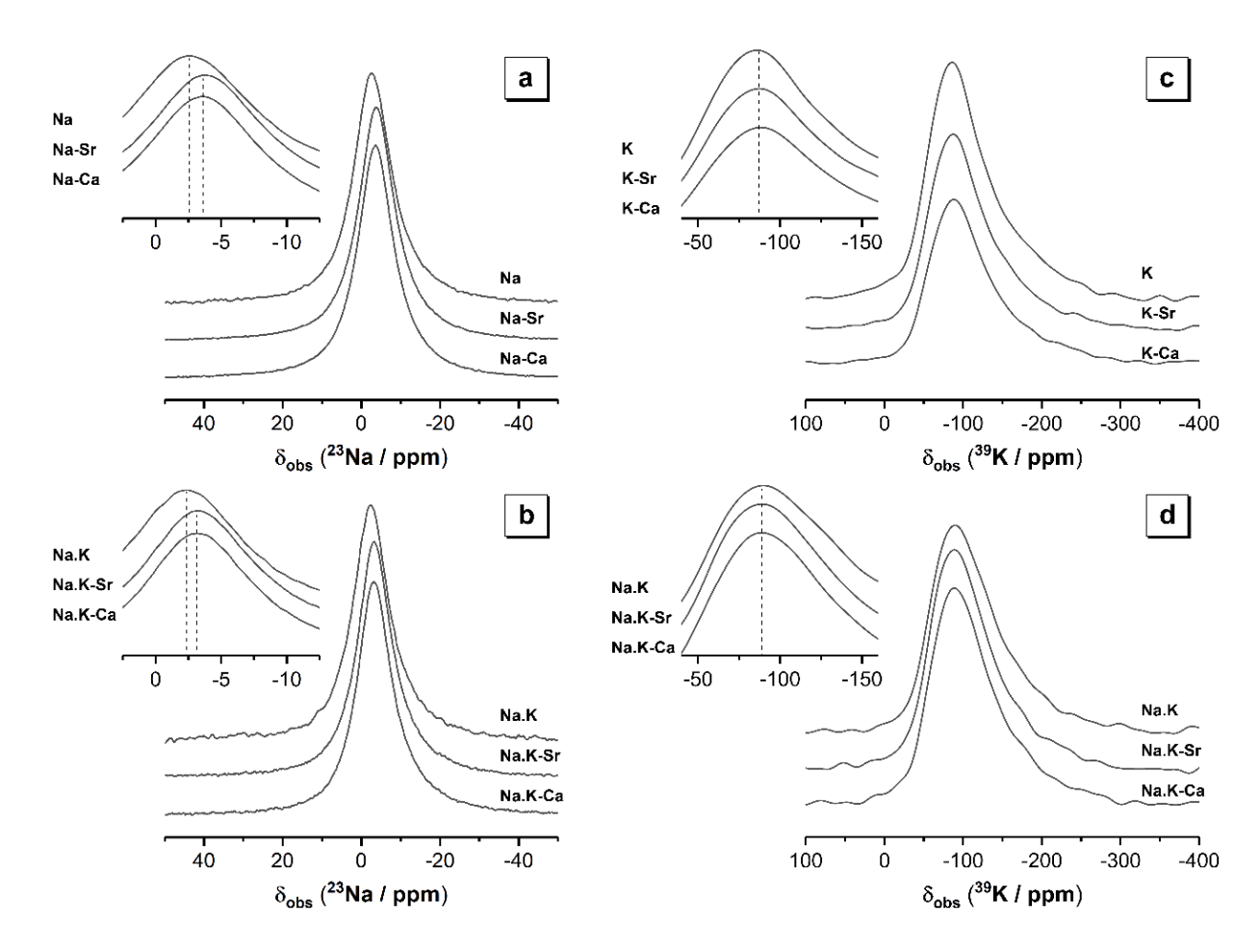


**Figure 9:** <sup>23</sup>Na MAS NMR spectra ( $B_0 = 11.7 \text{ T}$ ,  $v_R = 12.5 \text{ kHz}$ ) for geopolymers produced using a) sodium silicate and b) blended sodium-potassium silicate, and <sup>39</sup>K MAS NMR spectra ( $B_0 = 20.0 \text{ T}$ ,  $v_R = 12.0 \text{ kHz}$ ) for the geopolymers produced using c) potassium silicate and d) blended sodium-potassium silicate. The inset in each case shows a magnified region of the spectra.

# 3.2.1.4 X-ray absorption near-edge structure (XANES) spectroscopy

Normalised Sr X-ray absorption spectra for samples produced to assess the solubility limit of Sr within the N.K-A-S-H gels are shown in Figure 10 (Na-Sr 0.014 wt.%, Na.K Sr 0.014 wt.%, K-Sr 0.014 wt.%, Sr/Al = 0.00025). Data from standard compounds of  $SrCO_3$  [44] and the mineral brewsterite-Sr,  $(Sr,Ba)_2Al_4Si_{12}O_{32}\cdot10H_2O$ , [45] are overlaid for comparison.

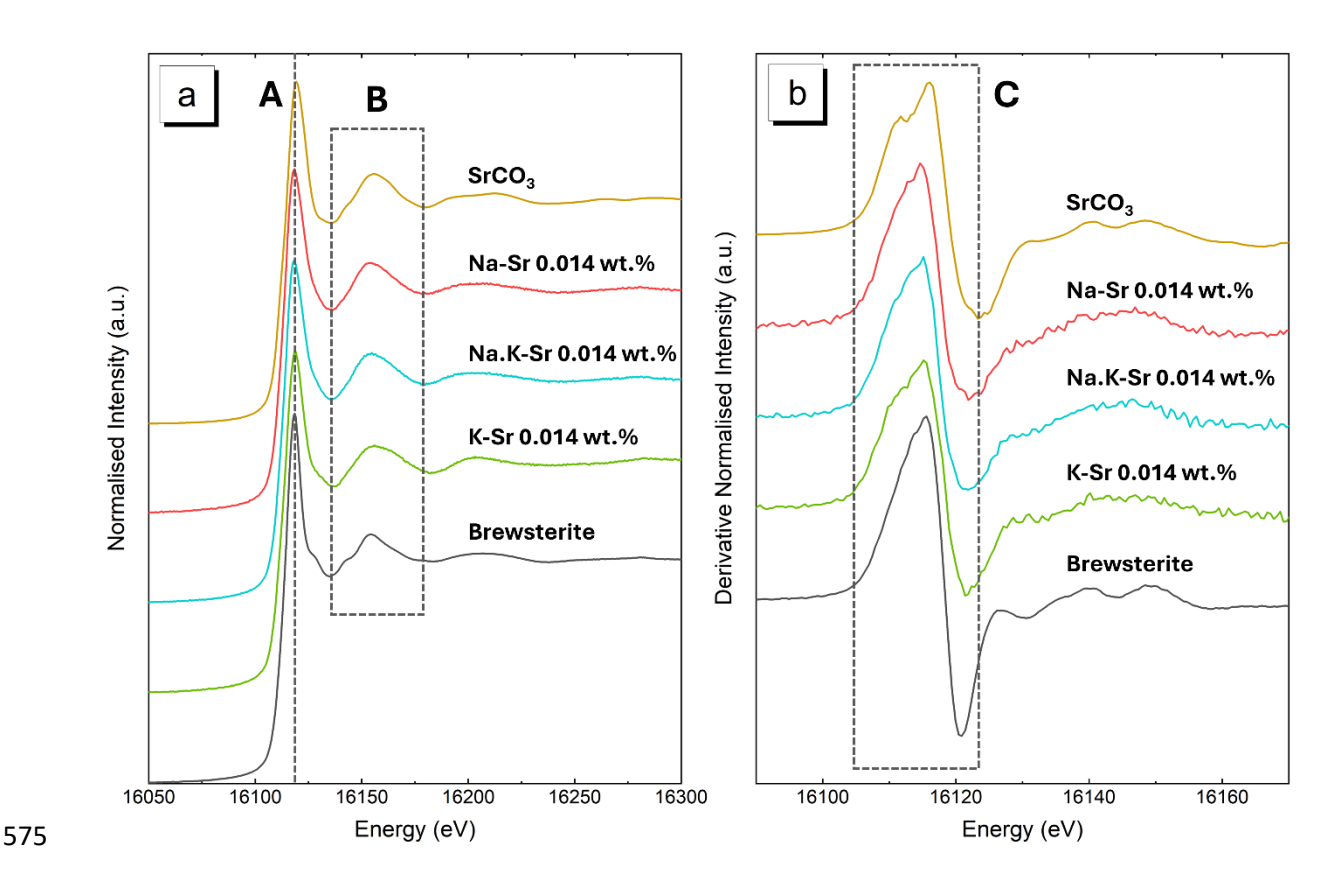


**Figure 10:** Normalised X-ray absorption spectra for the Sr-doped geopolymer samples. Overlaid are data from the mineral brewsterite-Sr and SrCO<sub>3</sub>. (b) 1st derivative of the spectra. The spectra have been stacked to improve clarity.

As previously discussed in Figure 5(a), the dotted line labelled A (Feature A) in Figure 10(a) shows a small shift of the maximum to the lower energy of brewsterite compared to SrCO<sub>3</sub>. However, the spectral features above the absorption edge are more difficult to match to either SrCO<sub>3</sub> or brewsterite (Feature B). This is likely due to the increased noise (Figure 10b, post 16130 eV) in the measurement of the Sr 0.014 wt. % samples, due to the presence of inherently less Sr. Despite this, when the 1<sup>st</sup> derivative energies of the samples are compared to the two standards (Figure 10b) a clear doublet (Feature C) is absent, indicative of SrCO<sub>3</sub>, as is present in the higher-loaded geopolymers. This indicates that Sr within the samples is structurally similar to brewsterite at the lower Sr loading (0.014 wt. %).

## 3.2.1.5 Extended X-ray Absorption Fine Structure (EXAFS)

Due to the similarities observed between the Sr 0.014 wt. % samples and brewsterite, a model was constructed utilising the brewsterite refinement reported by Artioli et al. [45]. The amplitude reduction factor and the refinement parameters of the three samples are reported in Table S4, Supporting Information. All three samples (Na, Na.K, K) were found to fit the brewsterite model with only minor adjustments from sample to sample. The model consists of a nearest neighbour oxygen shell, with a degeneracy of 7 to 9 (~2.6 Å) - Splitting of the first shell oxygen was attempted. However, this resulted in a less robust fit. Two further outer caution shells were present between 3.3 and 4.2 Å. As with the higher Sr-loaded geopolymers, the Si/Al path ratios were fixed at 2:1.5 to reflect the relevant elemental ratios in the samples. As an adaptive CIF file was used, mixed occupancy was not possible; hence, sites were selected as Si or Al. these limitations were considered while fitting the system as the mixed occupancy introduces disorder into the local structure, as the absorber is surrounded by a blend of Al and Si paths rather than distinct, well-defined paths represented in the CIF.

Progressing from Na to Na.K and K resulted in a gradual contraction of the O bond distances as is observed in Table S5, Supporting Information, and this was consistent with the observed reduction in N<sub>Sr-O</sub>, which indicates a decrease in the coordination of the first shell oxygen due to steric and energetic factors. While the Si/Al ratio for all three samples was fixed, for the Na.K and K samples, increasing the coordination number of the Al and Si paths resulted in a more robust fit. This is theorised to be due to the increased size of the K<sup>+</sup> cation - with respect to Na - introducing distortion into the framework, and lowering the number of oxygen atoms that can directly coordinate around Sr, but simultaneously create more space for second shell atoms (Al/Si) to coordinate at a greater distance. However, the authors acknowledge that this cannot be fully confirmed due to the inability to represent the structure in true mixed occupancy. This inability to ideally model mixed occupancy is also theorised to be the cause of the Sr-Al  $\sigma^2$  in the K sample being slightly greater in uncertainty than the value itself. Removing the Al path resulted in the best fit; however, despite Si being a stronger X-ray scatterer and in greater concentrations than AI, this difference should not be great enough to justify the removal of the path with the inclusion of Si at the same distance. As in the previous models, the BVS [52] was used as a restraint and returned values of 2.04  $\pm$  0.15, 2.03  $\pm$ 0.06 and 2.07  $\pm$ 0.07 v.u. for Na, Na.K, and K, respectively. The  $k^3$  weighted X(k) and FT, together with the fits to the structural model, are shown in Figure 2, Supporting Information. Attempts were made to fit the experimental results to SrCO<sub>3</sub>. However, these were unsuccessful, indicating that Sr is present in a pseudozeolitic framework.

#### 3.3 Mass transport properties of Sr during leaching

Plots showing cumulative leach fractions of Sr, Na, K, Al and Si in the leachate for geopolymer sample over time for the duration of the 28 day semi-dynamic leach test are provided in Figure 11. The concentration of Sr, Na, K, Al and Si within the leachate of each sample from the semi-dynamic leach tests was determined using ICP-OES. The cumulative fraction leached (CFL) of Sr, Na, K, Al and Si, can be calculated using Equation 1, where  $a_n$  is the mass of the species released during the leaching time interval n, and  $A_0$  is the total mass of the species in the sample at the start of the leach test.

$$CFL = \frac{\sum a_n}{A_0} \tag{1}$$

The incremental concentration (mg/mL) of Sr present in the leachate for each sample was greatest between 2 and 24h after leaching commences, after which it decreases significantly. During this stage Sr leaching primarily results from surface wash-off and rapid diffusion of aqueous Sr<sup>2+</sup> cations from the geopolymer gel surface and pore solution. Similar 'surface wash-off' effects have been observed previously for <sup>137</sup>Cs and <sup>60</sup>Co leaching from cements [56, 57]. The subsequent rapid decrease in the incremental concentrations of Sr, down to very low levels beyond 7-14 days of leaching, indicates a significant decrease in the rate of Sr release, and suggests significant hindrance of mass transport of Sr between 24 hours and 28 days. The behaviour of Na<sup>+</sup> and K<sup>+</sup> initially follows similar trends to those observed for Sr<sup>2+</sup>, but the release of these elements continues at a significant rate throughout the duration of the leaching experiments, without showing the much more marked deceleration observed in the Sr<sup>2+</sup> data. Overall, across all amounts of Sr incorporation investigated (1, 2, and 3 wt. % Sr), the potassium silicate-based geopolymers exhibit significantly less leaching of Sr when compared to sodium silicate-based geopolymers.

Incorporation of Sr also affects the extent of leaching of Na, K, Al, and Si. In all samples, the extent of leaching of Al and Si is increases with the amount of Sr incorporated in the sample. Overall, the potassium silicate-based geopolymers exhibited significantly less Al and Si leaching when compared to sodium silicate-based geopolymers, with the CFL values for Al and Si being approximately half of those for Nageopolymers. The values and variation in Al and Si leaching are extremely low, with the maximum CFL values for Al and Si observed across all samples being 0.20% and 0.35%, respectively (sample Na\_3%). An increased content of Sr resulted in a less rapid deceleration of Al and Si leaching. The CFL value for Sr in all samples is extremely low, with the maximum CFL for Sr observed across all samples being 0.013% (sample Na\_3%); the CFL for Sr is two orders of magnitude smaller than for Al and Si, and three orders of

magnitude smaller than the alkali cations, indicating preferential binding of Sr over alkali cations that are competing for the same charge-balancing sites within the N-A-S-H gel framework.

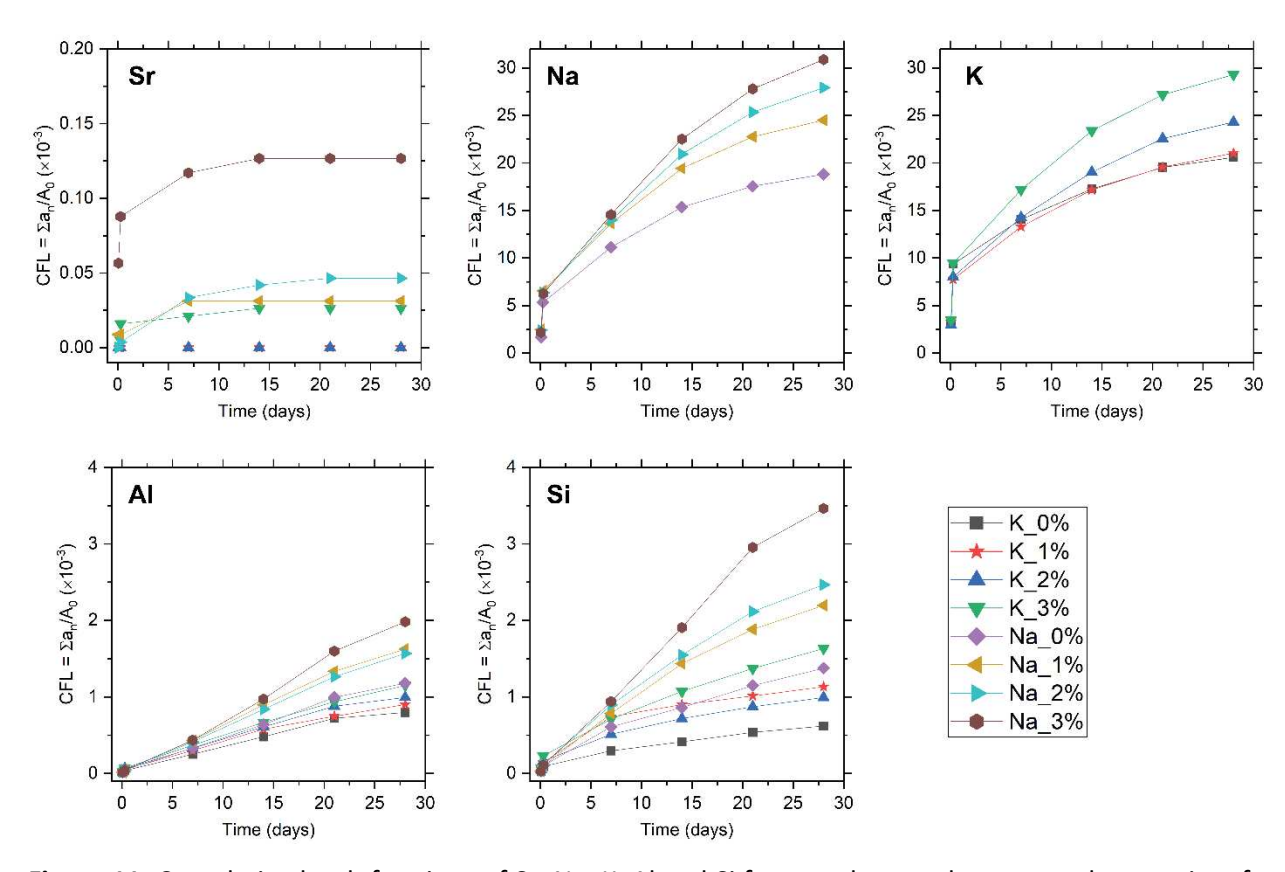


**Figure 11:** Cumulative leach fractions of Sr, Na, K, Al and Si from each geopolymer sample over time for the duration of the 28 day semi-dynamic leach test.

#### 4 Conclusions

The effect of alkali-activator chemistry and the addition of Sr on the chemistry, phase assemblage and nanostructure, and incorporation mechanism of  $Sr^{2+}$  into the aluminosilicate framework of (N,K)-A-S-H gels in geopolymers was investigated by 1) incremental addition of up to 3.5 wt.%  $Sr(OH)_2.8H_2O$  to sodium silicate-activated metakaolin-based geopolymers, and 2) addition of 0.014 wt. %  $Sr(OH)_2.8H_2O$  to metakaolin-based geopolymers produced using sodium silicate, potassium silicate, or a blend of sodium-and potassium-silicate. The main reaction product in all geopolymers was a fully polymerised, X-ray amorphous Al-rich (N,K)-A-S-H-type gel. Si exists predominantly in tetrahedral  $Q^4(4AI)$  and  $Q^4(3AI)$  sites and Al exists in tetrahedrally coordinated sites, resulting in a net negative charge that is balanced by  $Na^+$  and/or  $K^+$  in extra-framework sites. In geopolymers produced using both sodium silicate and potassoium silicate, and a mixture of both, and containing 0.014 wt. %  $Sr(OH)_2.8H_2O$ ,  $Sr^{2+}$  was incorporated into extra-framework sites within the N-A-S-H gels by directly substituting for  $Na^+$  and  $K^+$  in charge-balancing sites to form a (N,K,Sr)-A-S-H gel.

Formation of SrCO<sub>3</sub> was observed for geopolymers containing  $\geq 1.0$  wt. % Sr(OH)<sub>2</sub>·8H<sub>2</sub>O. The local structure of Sr in geopolymers containing 0.014 wt. % Sr(OH)<sub>2</sub>·8H<sub>2</sub>O (molar Sr/Al = 0.00025) was consistent with Sr atoms adopting structural positions within cavities in a pseudo-zeolitic framework structure similar to that of the natural zeolite brewsterite-Sr, (Sr,Ba)<sub>2</sub>Al<sub>4</sub>Si<sub>12</sub>O<sub>32</sub>·10H<sub>2</sub>O. In geopolymers loaded with 1.0, 2.0, and 3.0 wt. % Sr(OH)<sub>2</sub>·8H<sub>2</sub>O (molar Sr/Al = 0.018, 0.035, and 0.053, respectively) Sr exhibited a local structure similar to SrCO<sub>3</sub>. This shows that the limit for chemical immobilisation of Sr<sup>2+</sup> in geopolymers is equal to or below Sr/Na = 0.005 (0.5 mol.% of monovalent Na replaced by divalent Sr, equivalent to 0.5 wt. % Sr(OH)<sub>2</sub>·8H<sub>2</sub>O in the geopolymer formulation). The mechanisms controlling this may be related to the extent to which the local gel structure can accommodate charge balancing cations with different valances ionic radii, or may be due thermodynamically or kinetically preferential formation of SrCO₃ compared to (N,Sr)-A-S-H under the reaction conditions used. The geopolymers simultaneously chemically bind Sr within a (N,Sr)-A-S-H gel, and physically encapsulate excess Sr as SrCO<sub>3</sub>, at waste loadings above those which result in Sr/Na = 0.005. Potassium silicate-based geopolymers exhibit significantly less leaching of Sr when compared to sodium silicate-based geopolymers. Incorporation of Sr also affects the extent of leaching of Na, K, Al, and Si. In all samples, the extent of leaching of Al and Si is increases with the amount of Sr incorporated in the sample

The findings presented here significantly advance the understanding of the incorporation mechanism and chemical binding capacity of Sr-bearing geopolymers. This new insight is critical to support further

research into geopolymers for encapsulation and/or immobilisation of radioactive waste containing strontium-90, particularly given recent focus on potassium silicate-based geopolymers in the nuclear waste management sector due to their lower viscosity and desirable flow characteristics when compared with sodium silicate-based geopolymers.

# 5 Acknowledgements

This work has been funded by the Engineering and Physical Sciences Research Council (EPSRC), UK, through grants EP/P013171/1 and EP/Y029208/1. The UK 850 MHz solid state NMR Facility used in this work was funded by EPSRC and BBSRC (grant EP/T015063/1), as well as the University of Warwick, including via part funding through Birmingham Science City Advanced Materials Projects 1 and 2 supported by Advantage West Midlands (AWM), and the European Regional Development Fund (ERDF). We acknowledge Diamond Light Source for time on Beamline B18 under Proposal SP23343-2, and thank Dr Giannantonio Cibin, Principal Beamline Scientist, B18, Diamond Light Source, for assistance with acquiring the XAS data. We thank and acknowledge Dr Sandra van Meurs, Department of Chemistry, The University of Sheffield, for assistance in acquiring some of NMR data obtained at The University of Sheffield, Dr Oday Hussein, Department of Materials Science and Engineering, The University of Sheffield, for assistance in acquiring the FTIR data. Aspects of this work utilised the HADES/MIDAS facility at The University of Sheffield, established with financial support from EPSRC and BEIS (grant EP/T011424/1). We are also very grateful to the PQ Corporation for the provision of alkali silicate solutions for this experimental programme.

### References

- 708 1. Qian, G., et al., *Improvement of metakaolin on radioactive Sr and Cs immobilization of alkali-*709 *activated slag matrix.* Journal of Hazardous Materials, 2002. **92**(3): p. 289-300.
- 710 2. Ochs, M., D. Mallants, and L. Wang, *Radionuclide and Metal Sorption on Cement and Concrete*. 711 2015, Switzerland: Springer International Publishing.
- 712 3. Kuenzel, C., et al., *Encapsulation of Cs/Sr contaminated clinoptilolite in geopolymers produced* 713 *from metakaolin.* Journal of Nuclear Materials, 2015. **466**: p. 94-99.
- 714 4. Oh, S., et al. Homogeneity Evaluation for Geopolymer Waste Form with Spent Ion-exchange 715 Resin. in Transactions of the American Nuclear Society. 2024.
- 5. Shin, Y., et al., Estimation of radionuclides leaching characteristics in different sized geopolymer
   waste forms with simulated spent ion-exchange resin. Nuclear Engineering and Technology,
   2023. 55(10): p. 3617-3627.
- Tusa, E., Cesium and strontium removal with highly selective ion exchange media in Fukushima
   and cesium removal with less selective media-14018, in Waste Management Symposia. 2014:
   Phoenix, Arizona, USA.
- 722 7. Wieland, E., et al., *Strontium uptake by cementitious materials*. Environmental Science & Technology, 2008. **42**(2): p. 403-409.
- 724 8. Tits, J., et al., *Strontium binding by calcium silicate hydrates*. Journal of Colloid and Interface Science, 2006. **300**(1): p. 78-87.
- Mukiza, E., et al., Co-immobilization of cesium and strontium containing waste by metakaolin based geopolymer: Microstructure, mineralogy and mechanical properties. Journal of Nuclear
   Materials, 2023. 585.
- 729 10. Jain, S., et al., Advancements in immobilization of cesium and strontium radionuclides in cementitious wasteforms—A review. Journal of the American Ceramic Society, 2025. **108**(1).
- 731 11. Niu, X., et al., Adsorption behaviour of simulant radionuclide cations and anions in metakaolin-732 based geopolymer. Journal of Hazardous Materials, 2022. **429**: p. 128373.
- 733 12. Arbel Haddad, M., et al., *Formation of zeolites in metakaolin-based geopolymers and their*734 *potential application for Cs immobilization.* Journal of Nuclear Materials, 2017. **493**: p. 168-179.
- 735 13. Williams, B.D., et al., *Mineral assemblage transformation of a metakaolin-based waste form* 736 *after geopolymer encapsulation.* Journal of Nuclear Materials, 2016. **473**: p. 320-332.
- 737 14. Provis, J.L., P.A. Walls, and J.S.J. van Deventer, *Geopolymerisation kinetics. 3. Effects of Cs and Sr salts.* Chemical Engineering Science, 2008. **63**(18): p. 4480-4489.
- 739 15. Ofer-Rozovsky, E., et al., *Cesium immobilization in nitrate-bearing metakaolin-based* 740 *geopolymers.* Journal of Nuclear Materials, 2019. **514**: p. 247-254.
- 741 16. Provis, J.L., A. Palomo, and C.J. Shi, *Advances in understanding alkali-activated materials*. 742 Cement and Concrete Research, 2015. **78**: p. 110-125.
- 743 17. Provis, J.L., et al., *Statistical thermodynamic model for Si/Al ordering in amorphous aluminosilicates.* Chemistry of Materials, 2005. **17**(11): p. 2976-2986.
- 745 18. Walkley, B., et al., *Incorporation of strontium and calcium in geopolymer gels.* Journal of Hazardous Materials, 2020. **382**: p. 121015.
- 747 19. Kirishima, A., T. Sasaki, and N. Sato, *Solution chemistry study of radioactive Sr on Fukushima Daiichi NPS site.* Journal of Nuclear Science and Technology, 2015. **52**(2): p. 152-161.
- 749 20. Koma, Y., A. Shibata, and T. Ashida, *Radioactive contamination of several materials following the* 750 *Fukushima Daiichi Nuclear Power Station accident.* Nuclear Materials and Energy, 2017. 10: p.
   751 35-41.

- 752 21. Blackford, M.G., et al., *Transmission electron microscopy and nuclear magnetic resonance* 753 studies of geopolymers for radioactive waste immobilization. Journal of the American Ceramic 754 Society, 2007. **90**(4): p. 1193-1199.
- Perera, D.S., et al., *Immobilization of Cs and Sr in geopolymers with Si/Al molar ratio of*  $\sim$  2. Ceramic Transactions, 2006. **176**: p. 91-96.
- 757 23. Xu, Z., et al., *Immobilization of strontium-loaded zeolite A by metakaolin based-geopolymer*.
  758 Ceramics International, 2017. **43**(5): p. 4434-4439.
- 759 24. Ke, X., et al., *Alkali aluminosilicate geopolymers as binders to encapsulate strontium-selective titanate ion-exchangers.* Dalton Transactions, 2019. **48**(32): p. 12116-12126.
- Soonthornwiphat, N., et al., Encapsulation of Sr-loaded titanate spent adsorbents in potassium
   aluminosilicate geopolymer. Journal of Nuclear Science and Technology, 2020. 57(10): p. 1181 1188.
- 764 26. Ismail, I., et al., *Drying-induced changes in the structure of alkali-activated pastes.* Journal of Materials Science, 2013. **48**(9): p. 3566-3577.
- 766 27. American National Standard Measurement of the Leachability of Solidified Low-Level Radioactive 767 Wastes by a Short-Term Test Procedure. 2003, American Nuclear Society: Illinois.
- 768 28. Harris, R.K., et al., NMR Nomenclature: Nuclear Spin Properties and Conventions for Chemical
   769 Shifts: IUPAC Recommendations 2001. Solid State Nuclear Magnetic Resonance, 2002. 22(4): p.
   770 458-483.
- 771 29. Massiot, D., et al., *Modelling one- and two-dimensional solid-state NMR spectra*. Magnetic Resonance in Chemistry, 2002. **40**(1): p. 70-76.
- 773 30. Ravel, B. and M. Newville, *ATHENA, ARTEMIS, HEPHAESTUS: data analysis for X-ray absorption*774 *spectroscopy using IFEFFIT.* Journal of synchrotron radiation, 2005. **12**(4): p. 537-541.
- White, C.E., et al., Combining density functional theory (DFT) and pair distribution function (PDF)
   analysis to solve the structure of metastable materials: the case of metakaolin. Physical
   Chemistry Chemical Physics, 2010. 12(13): p. 3239-3245.
- Wang, L., et al., *The role of zinc in metakaolin-based geopolymers.* Cement and Concrete Research, 2020. **136**: p. 106194.
- 780 33. Duxson, P., G.C. Lukey, and J.S.J. van Deventer, *Evolution of Gel Structure during Thermal* 781 *Processing of Na-Geopolymer Gels.* Langmuir, 2006. **22**(21): p. 8750-8757.
- 782 34. Provis, J.L., G.C. Lukey, and J.S.J. van Deventer, *Do geopolymers actually contain nanocrystalline zeolites? A reexamination of existing results.* Chemistry of Materials, 2005. **17**(12): p. 3075-3085.
- Alavi, M.A. and A. Morsali, Syntheses and characterization of Sr(OH)₂ and SrCO₃ nanostructures
   by ultrasonic method. Ultrasonics Sonochemistry, 2010. 17(1): p. 132-138.
- 786 36. Duxson, P., et al., <sup>29</sup>Si NMR study of structural ordering in aluminosilicate geopolymer gels. 787 Langmuir, 2005. **21**(7): p. 3028-36.
- 788 37. Walkley, B., et al., *Phase evolution of Na<sub>2</sub>O-Al<sub>2</sub>O3-SiO<sub>2</sub>-H<sub>2</sub>O gels in synthetic aluminosilicate* binders. Dalton Transactions, 2016. **45**(13): p. 5521-35.
- Jonghi, M.A., et al., Metakaolin-based geopolymers: Relation between formulation,
   physicochemical properties and efflorescence formation. Composites Part B: Engineering, 2020.
   182: p. 107671.
- 793 39. Engelhardt, G., et al., <sup>29</sup>Si-NMR-Untersuchungen zur Verteilung der Silicium-und 794 Aluminiumatome im Alumosilicatgitter von Zeolithen mit Faujasit-Struktur. Zeitschrift für 795 anorganische und allgemeine Chemie, 1981. **482**(11): p. 49-64.
- 796 40. Walkley, B., et al., *New structural model of hydrous sodium aluminosilicate gels and the role of* 797 *charge-balancing extra-framework Al.* Journal of Physical Chemistry C, 2018. **122**(10): p. 5673-798 5685.

- 799 41. Duxson, P., et al., *Effect of alkali cations on aluminum incorporation in geopolymeric gels.* 800 Industrial & Engineering Chemistry Research, 2005. **44**(4): p. 832-839.
- Kobera, L., et al., Biaxial Q-shearing of <sup>27</sup>Al 3QMAS NMR spectra: Insight into the structural disorder of framework aluminosilicates. Solid State Nuclear Magnetic Resonance, 2014. 57–58:
   p. 29-38.
- 804 43. Stebbins, J.F., et al., *Quantification of five- and six-coordinated aluminum ions in aluminosilicate*805 and fluoride-containing glasses by high-field, high-resolution <sup>27</sup>Al NMR. Journal of Non806 Crystalline Solids, 2000. **275**(1–2): p. 1-6.
- 807 44. Pannhorst, W. and J. Löhn, *Zur Kristallstruktur von Strontianit, SrCO3.* Zeitschrift für Kristallographie Crystalline Materials, 1970. **131**(1-6): p. 455-459.
- 45. Artioli, G., J.V. Smith, and Å. Kvick, *Multiple hydrogen positions in the zeolite brewsterite*,(*Sr0. 95, Ba0. 05*) *Al2Si6O16. 5H2O.* Acta Crystallographica Section C: Crystal Structure

  811 Communications, 1985. **41**(4): p. 492-497.
- Joseph, K., et al., *Iron phosphate glasses: Bulk properties and atomic scale structure.* Journal of
   Nuclear Materials, 2017. 494: p. 342-353.
- Waychunas, G.A., M.J. Apted, and G.E. Brown, *X-ray K-edge absorption spectra of Fe minerals* and model compounds: Near-edge structure. Physics and Chemistry of Minerals, 1983. **10**(1): p. 1-9.
- Wilke, M., et al., *Oxidation state and coordination of Fe in minerals: An Fe K-XANES spectroscopic study.* American Mineralogist, 2001. **86**(5-6): p. 714-730.
- 819 49. Farges, F., et al., *The effect of redox state on the local structural environment of iron in silicate*820 *glasses: a combined XAFS spectroscopy, molecular dynamics, and bond valence study.* Journal of
  821 Non-Crystalline Solids, 2004. **344**(3): p. 176-188.
- Kelly, S.D., D. Hesterberg, and B. Ravel, *Analysis of Soils and Minerals Using X-ray Absorption Spectroscopy*, in *Methods of Soil Analysis Part 5—Mineralogical Methods*. 2008. p. 387-463.
- Li, G.G., F. Bridges, and C.H. Booth, *X-ray-absorption fine-structure standards: A comparison of experiment and theory.* Physical Review B, 1995. **52**(9): p. 6332-6348.
- 826 52. Brown, I.D., *Recent Developments in the Methods and Applications of the Bond Valence Model.*827 Chemical Reviews, 2009. **109**(12): p. 6858-6919.
- Gagné, O.C. and F.C. Hawthorne, Comprehensive derivation of bond-valence parameters for ion pairs involving oxygen. Acta Crystallographica Section B: Structural Science, Crystal Engineering and Materials, 2015. 71(5): p. 562-578.
- Chitsaz, S. and A. Tarighat, Molecular dynamics simulation of N-A-S-H geopolymer macro
   molecule model for prediction of its modulus of elasticity. Construction and Building Materials,
   2020. 243: p. 118176.
- Duxson, P., et al., <sup>39</sup>K NMR of free potassium in geopolymers. Industrial and Engineering Chemistry Research, 2006. **45**: p. 9208-9210.
- 836 56. Komljenović, M., et al., *Immobilization of cesium with alkali-activated blast furnace slag.* Journal of Hazardous Materials, 2020. **388**: p. 121765.
- Abdel Rahman, R.O. and A.A. Zaki, *Assessment of the leaching characteristics of incineration ashes in cement matrix.* Chemical Engineering Journal, 2009. **155**(3): p. 698-708.

840